Environmental controls on crenarchaeol distributions in hydrothermal springs

Amanda N. Calhoun[1,2,*], Jerome Blewett[2,#], Daniel R. Colman[3], Maximiliano J. Amenabar[3,@], Carolynn M. Harris[1], Eric S. Boyd[3], Ann Pearson[2], William D. Leavitt[1,4,5*]

(1) Department of Earth Sciences, Dartmouth College, Hanover, NH, USA
(2) Department of Earth & Planetary Sciences, Harvard University, Cambridge, MA, USA
(3) Department of Microbiology & Immunology, Montana State University, Bozeman, MT, USA
(4) Department of Chemistry, Dartmouth College, Hanover, NH, USA
(5) Department of Geology & Geophysics, University of Utah, Salt Lake City, UT

*Correspondence: acalhoun@g.harvard.edu; Wil.Leavitt@dartmouth.edu ;

#Current Affiliation: Department for Energy Security and Net Zero, London, UK
@Current Affiliation: Escuela de Biotecnología, Facultad de Ciencias, Universidad Santo Tomás, Chile

Keywords: hot springs; archaeal lipids; biomarkers; aqueous geochemistry

ABSTRACT

Thermophilic archaea synthesize cellular membranes composed primarily of isoprenoid glycerol dibiphytanyl glycerol tetraethers (iGDGTs). Cells can adjust the structure of iGDGTs by increasing the number of cyclopentyl rings to enhance lipid packing, thereby decreasing membrane permeability and fluidity to maintain cellular function at high temperature and/or acidic pH. Certain archaea synthesize an iGDGT, crenarchaeol, with four cyclopentyl rings and a unique cyclohexyl ring, the function of which is unknown. Structural modeling suggests the cyclohexyl ring may increase membrane fluidity, potentially representing an adaptation that allowed thermophiles to radiate into cooler environments. To begin to investigate this hypothesis, iGDGT abundance was quantified in forty-one hydrothermal springs in Yellowstone National Park (YNP), USA, and contextualized within a compilation of global hydrothermal spring iGDGTs with pH values of 1.1 to 10.1 and temperatures of 16.3 to 95 °C. pH most strongly correlated with both crenarchaeol abundance and the number of cyclopentyl rings per iGDGT. Crenarchaeol abundance exhibited a nonlinear relationship with both pH and temperature, with highest abundances at pH 7.4 and 46 °C, then decreasing in abundance above and below these values. These observations support the hypothesis that crenarchaeol's cyclohexyl ring facilitated the adaptation of thermophilic and acidophilic archaea to lower temperature and higher pH niches, enabling their radiation into the marine realm.

IMPORTANCE

Archaea change the composition of their membrane lipids to alter the fluidity of their membranes to protect cellular functions from environmental stressors. Some archaea produce a lipid, crenarchaeol, with a unique six-membered ring, the effect of which on archaeal membrane dynamics remains unknown. In this study, we identify pH as the most important geochemical variable for archaeal membrane response in Yellowstone National Park hot springs. In addition, the lipid distributions we find support the hypothesis that crenarchaeol facilitated the archaeal evolutionary transition from hot and acidic to cool and neutral waters. We contextualize these findings in a literature compilation that spans the globe.

1. INTRODUCTION

Terrestrial hydrothermal systems are valuable analogs of early Earth environments where many origins of life theories suggest life first emerged due to sharp thermal and geochemical gradients (Damer and Deamer, 2020). Archaea are ubiquitous in these environments and are adapted to the extreme conditions within these systems that impose chronic energy stress (Valentine, 2007; van de Vossenburg et al., 1998; Macalady et al., 2004; Schouten et al., 2013). A primary adaptation in archaea that inhabit extreme geothermal environments is the structural properties of their isoprenoid glycerol dibiphytanyl glycerol tetraether (iGDGT) lipids that comprise their cell membranes (Konings et al., 2002; van de Vossenberg et al., 1998). Archaeal iGDGTs are also ubiquitous in soils, lakes, marine waters, and sediments, where they can serve as paleoenvironmental proxies (Schouten et al., 2002; Schouten et al., 2000; Schouten et al., 2013). Interactions between archaea and their environments have shaped their adaptation and evolution (Colman et al., 2018; Yang et al., 2021), specifically the adjustment of cell membrane fluidity and permeability in response to physical and chemical stressors (Oger and Cario, 2013).

The membranes of thermophilic and acidophilic archaea are primarily composed of iGDGTs (Macalady et al., 2004; Oger and Cario, 2013). These molecules vary in the number of cyclopentane or cyclohexane rings present in their internal biphytanyl chains (De Rosa and Gambacorta, 1980; De Rosa and Gambacorta, 1988; Schouten et al., 2000). The rings in iGDGTs affect molecular packing (Figure 1), enabling the modulation of archaeal cell membrane fluidity and permeability in response to changing temperature, pH, energy stress, salinity, and pressure through production of more or fewer rings as needed (Gabriel and Chong, 2000; Pearson and Ingalls, 2013; Albers et al., 2000; Zhou et al., 2020; Boyd et al., 2011; Feyhl-Buska et al., 2016). In most environments, archaea produce iGDGTs with zero to four cyclopentane rings (iGDGT-0 to iGDGT-4), but in hydrothermal springs, archaea can produce iGDGTs with up to eight cyclopentane rings (iGDGT-8) (Pancost et al., 2006; Schouten et al., 2013). The increase in average ring counts of iGDGTs at higher temperatures is the basis for the TEX_{86} (TetraEther indeX of 86 carbon atoms) paleotemperature proxy (Schouten et al., 2002). However, recent studies indicate that

additional environmental parameters can influence cyclopentyl ring abundance, complicating the interpretation of TEX_{86} as a strict temperature proxy (Qin et al., 2015; Elling et al., 2015; Hurley et al., 2016; Zhou et al., 2020; Cobban et al., 2020; Tourte et al., 2022).

Crenarchaeol and its isomers are unique in that they contain a cyclohexane ring (Sinninghe Damsté et al., 2002). At present, the origin and synthetic mechanism of this ring remain unknown, while hypotheses on its physiological function are not yet well-established (Zhang et al 2006). While recent work has revealed many steps of iGDGT synthesis (e.g., Zeng et al., 2022; Lloyd et al., 2022), the biosynthetic pathway of iGDGT cyclohexyl rings remains elusive, leaving the natural history and function of crenarchaeol unknown. Crenarchaeol is thought to be specific to the phylum Nitrososphaerota (syn. Thaumarchaeota), which are ubiquitous in terrestrial hot springs, soils, and marine water columns, where they can be the most abundant nitrifiers (Ueda et al., 1995; Karner et al., 2001; Stahl and de la Torre, 2012). A subgroup known to produce crenarchaeol, the ammonia-oxidizing archaea (AOA), only represents a fraction of the

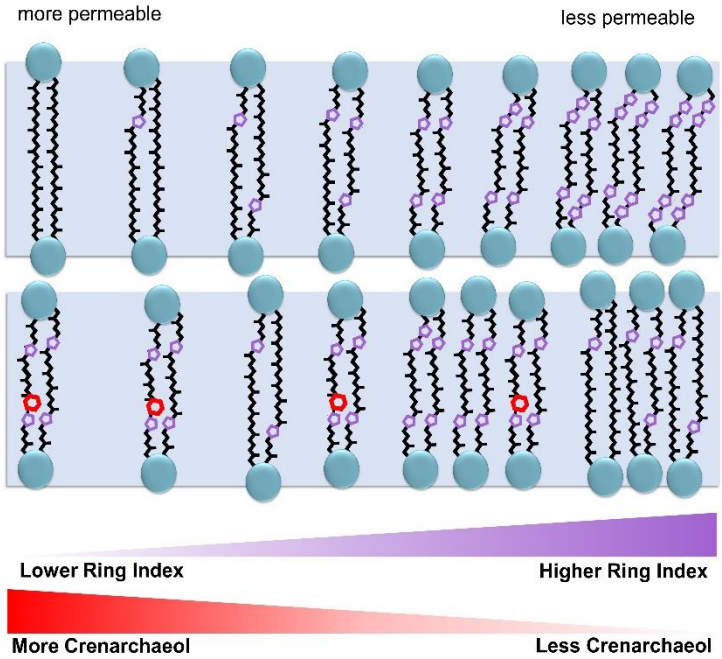

Figure 1. Schematic of effects of cyclopentyl rings (purple) on archaeal membrane permeability versus the hypothesized effect of cyclohexyl rings (red) on archaeal membrane permeability, indicated by lower bars.

often abundant Nitrososphaerota in hot springs (Colman et al., 2024). It is estimated that the crenarchaeol-producing AOA originated in terrestrial hot springs, then expanded their niche to the cooler and carbonate buffered waters of Earth's marine realm somewhere between 1017 million years ago (Ma; Ren et al., 2019) to 509 Ma (Yang et al., 2021). If this is true, the progenitor that was originally optimized to live at high temperatures (and perhaps low pH) had to adapt its membrane structure away from the dense, rigid membranes of hyperthermophilic archaea with high numbers of cyclopentyl rings. Incorporating crenarchaeol's cyclohexyl ring may have relaxed molecular packing in cellular membranes, facilitating the colonization of hyperthermophilic archaea in the less "extreme" marine realm (Schouten et al., 2000; Figure 1). This hypothesis is supported by lipid modeling that indicates the cyclohexane ring forms a bulge that increases biphytane volume, preventing dense membrane packing (Sinninghe-Damsté et al., 2002). A previous study suggested a 40 °C temperature optimum for crenarchaeol given its abundance normalized to GDGT-0 in marine sediments and hot spring microbial mats (Zhang et al., 2006), but crenarchaeol can also be dominant in cultured archaea at temperatures above 70 °C (de la Torre et al., 2008). Together, these observations imply that temperature is not the only determinant of crenarchaeol distributions. In hot springs, a clear negative correlation between crenarchaeol abundance and acidity (Boyd et al., 2013) implies that crenarchaeol is synthesized to a greater extent in circumneutral waters as opposed to acidic conditions.

Here we utilize lipid data to examine patterns of crenarchaeol abundance and distribution from 299 hot spring samples from North America, Europe, and Asia that span variable temperature (16.3 to 95 °C), pH (1.1 to 10.1), redox (-334 to 331 mV for a new Yellowstone National Park 41 sample subset), and other geochemical conditions. In parallel, we calculate the summary indicator of cyclopentyl ring abundance, Ring Index (RI). This approach enables us to re-evaluate potential archaeal adaptations to environmental stress, allowing for the examination of key geochemical factors that drive crenarchaeol abundance on the present and past Earth. This work provides evidence in favor of a role of crenarchaeol in facilitating the diversification of thermophilic archaea into more mesophilic environments, including lower temperature circumneutral waters.

2. METHODS

Field Measurements and Sample Collection

A total of 41 sediment samples, encompassing 38 individual springs, were collected over four field seasons between 2018-2022 in Yellowstone National Park, USA (permit #5544) (Figure 2). Water temperature (°C), pH, dissolved oxygen (DO) concentration, specific conductivity (SPC), and oxidation reduction potential (ORP) were measured in the field at the time of sampling using a YSI ProDSS meter calibrated for DO and with pH buffer solutions of 4, 7, and 10 or 1.68, 4, and 7 (YSI, Yellow Springs, OH, USA). Concentrations of dissolved sulfide ($\Sigma H_2S/HS^-/S^{2-}$) and Fe^{2+} were determined in the field with a portable Hach spectrophotometer (model DR2800) and Hach reagents (Hach Company, Loveland, CO, USA) following established protocols (Colman et al., 2016). Sulfide and Fe^{2+} concentrations were measured on water samples collected by a high-density polyethylene sampling staff (turbid water samples were filtered through pre-sterilized 0.22 µm Sterivex filters (EMD Millipore, Billerica, MA, USA)), while all other parameters were measured in situ near the site of sediment collection. Sediments were collected into sterile conical centrifuge tubes using the sampling staff, placed on dry ice in the field, then transferred to storage at -80 °C. Sediments were shipped frozen to Dartmouth College and stored at -80 °C until further processing.

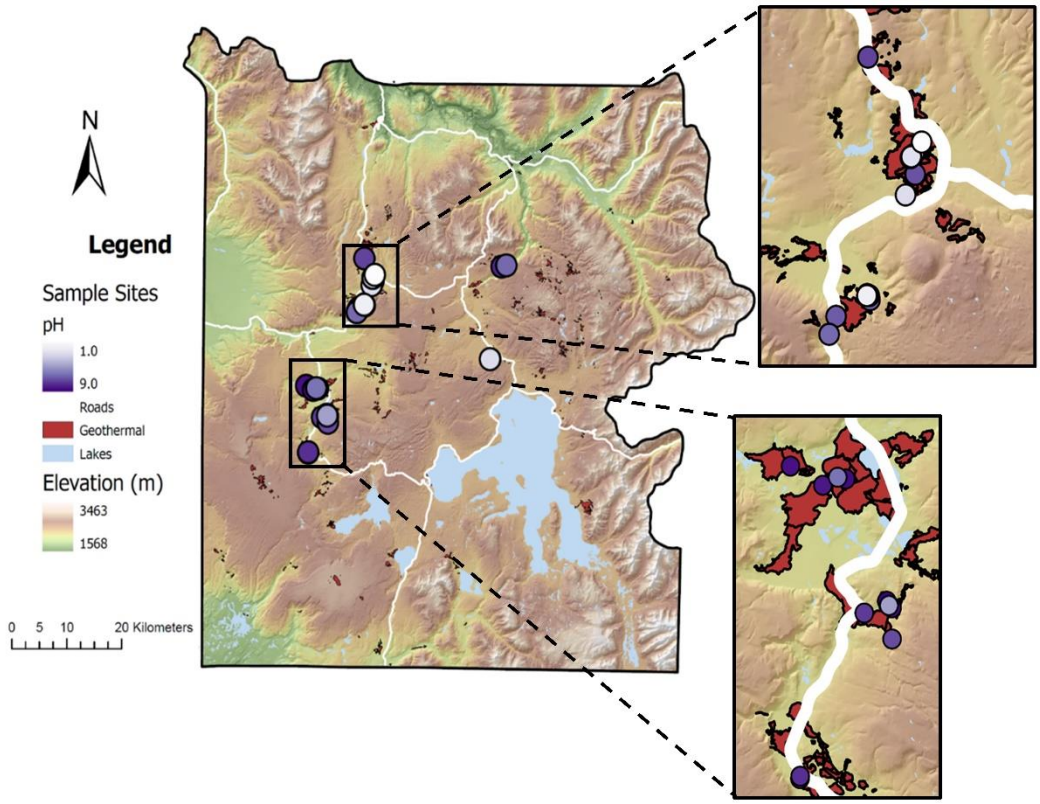

Figure 2. Map of sampling locations colored by pH in Yellowstone National Park, USA 2018 to 2022. Major roads are shown in white and geothermal areas are shaded in red.

Lipid Extraction and Preparation

Sediment samples were freeze-dried and stored at room temperature before extraction. Total lipid extracts (TLEs) were obtained by modified Bligh-Dyer extraction (Weber et al., 2017; Bligh and Dyer, 1959). Sediments (~1 g) were sonicated in 2:1:0.8 methanol:dichloromethane:trichloroacetic acid (MeOH:DCM:TCA) buffer (TCA, 50 g/L, pH = 2.1), centrifuged, and phase-extracted in four rounds. Organic phases underwent a final water rinse before concentration under N_2 gas and reconstitution in 2:1 DCM:methanol. Where necessary, multiple samples were merged for larger lipid yields (Table S1). TLEs were treated with activated (1 M HCl, rinsed with H_2O, MeOH, DCM, and hexane) copper at room temperature overnight to remove S^0 (Boyd et al., 2011). TLEs were separated into core lipid (CL) and intact polar lipid (IPL) fractions by solvent elution through SiO_2 columns as described in Pitcher et al. (2009) and stored in DCM at -20 °C. The polar headgroups of IPL fractions were cleaved (5% HCl in

MeOH, 3 hr). IPL-derived lipids were brought to a pH of 4 to 5 using 1 M KOH in MeOH, followed by four rounds of liquid-liquid extraction. CL- and IPL-derived lipid fractions were reconstituted in a mixture of 99:1 hexane:isopropyl alcohol (IPA) with addition of 100 ng of C_{46}-GTGT internal standard (Huguet et al., 2006). All samples were filtered through 0.45 µm PTFE filters (4 mm diameter) before analysis.

GDGT Quantification

All iGDGT fractions were analyzed by ultra-high performance liquid chromatography – atmospheric pressure chemical ionization – mass spectrometry (UHPLC-ACPI-MS) using an Agilent 1290 Infinity series UHPLC system coupled to an Agilent 6460 triple-quadrupole mass spectrometer (QQQ MS), consistent with methods used in earlier work (Zhou et al., 2020; Blewett et al., 2020). GDGTs were separated by injecting 10 µL of sample onto two coupled ACQUITY UPLC BEH Amide Columns (1.7 µm, 2.1 x 150 mm) held at 50 °C (Becker et al., 2013) with a constant solvent flow rate (0.5 mL/min) and solvent mixtures A (pure hexane), B (90:10 hexane:IPA), and D (30:70 MeOH:IPA). The program started at 98:2 A:B with a linear gradient to 3% B by 4 minutes, 10% B by 10 minutes, 20% B by 20 minutes, 50% B by 35 minutes, and 100% B by 40 minutes followed by a one-minute hold. At 41.01 minutes, the program was set to 70:30 B:D, ramping to 100:0 B:D by 46 minutes and 98:2 A:B by 47 minutes, holding until the total run time of 65 minutes. The QQQ-MS was operated in single ion monitoring (SIM) mode with a dwell time of 128 ms and fragmentor voltage of 75 V. GDGT relative abundances were determined by manual integration of ion chromatograms with mass to charge ratios (*m*/*z*) starting at 1302.3 for iGDGT-0 and decreasing by increments of 2 down to 1286.3 *m*/*z* for iGDGT-8.

Data Reduction and Statistical Analyses

Two RI values were calculated: with and without crenarchaeol (Eq. 1 and 2). In the numerator, the relative abundance of each lipid is multiplied by the number of cyclopentyl rings in the lipid structure (Zhang et al., 2016; Taylor et al., 2013). For this reason, crenarchaeol is incorporated as a four-ringed member in Equation 1 because the fifth ring is the enigmatic cyclohexyl ring whose contribution to

membrane dynamics is so far unconstrained (Zhang et al., 2016). See the Supplement for a discussion of the merits and drawbacks of including crenarchaeol as a four-ringed contributor to RI; we conclude that it is appropriate to exclude crenarchaeol from RI calculations if the intended purpose is to investigate membrane permeability.

$$RI_{(+cren)} = \left[\frac{G1+2*G2+3*G3+4*(G4+Cren+Cren')+5*G5+6*G6+7*G7+8*G8}{G0+G1+G2+G3+G4+Cren+Cren'+G5+G6+G7+G8}\right] \quad (1)$$

$$RI_{(-cren)} = \left[\frac{G1+2*G2+3*G3+4*G4+5*G5+6*G6+7*G7+8*G8}{G0+G1+G2+G3+G4+G5+G6+G7+G8}\right] \quad (2)$$

Given that neutral pH varies with temperature, we calculated the temperature-dependent neutral pH, i.e., the neutrality line, from 0 to 100 °C (Eq. 3; Justnes et al., 2020).

$$Neutral\ pH = 8 * (T^2 * 10^{-5}) - (0.0208 * T) + 7.4692 \quad (3)$$

Statistical analyses were performed using R Statistical Software (v4.4.0; R Core Team, 2024). Scripts for statistical runs and plots are available at https://zenodo.org/doi/10.5281/zenodo.12603497. Quadratic and interaction terms were tested in modelling, but these were not substantially more powerful than reported models. All input variables of regression models are normalized using the base *scale*() function of R to prevent skew due to parameter magnitude.

3.0 Results

3.1 Lipid characteristics among YNP hydrothermal springs

Geochemical parameters for the YNP samples collected in this study (N = 41; Supplement Table S1) include temperature (28.2 to 92.8 °C), pH (1.14 to 9.02), dissolved oxygen (DO; 0.005 to 1.99 mg/L), specific conductivity (SPC; 48 to 5380 µS/cm), oxidation reduction potential (ORP; -334 to 330.8 mV),

Fe^{2+} (0 to 1.97 mg/L) and dissolved sulfide (S^{2-}; 0 to 7858 µg/L) concentrations. None of these parameters were normally distributed, so Spearman's rho correlations were used to evaluate their relationships with lipid characteristics. The relationships between these environmental variables, crenarchaeol abundance, and Ring Index (see Table S1 for individual site values) were calculated using simple (SLR) and multiple linear regressions (MLR) of all possible geochemical parameter combinations that were performed on both CL and IPL fractions. Model results reported below are for CL fractions and statistical results for both fractions are compared in the Supplemental Information (Tables S2, S3, S5, S6). The RI results reported here include crenarchaeol as a four-ringed member, as seen in previous studies (Zhang et al., 2016).

The non-linear Spearman's rho tests demonstrated that pH and Fe^{2+} concentration were the only variables that were significantly associated with CL and IPL crenarchaeol relative abundance for the 41 new YNP samples (Table S2). However, significant relationships between Fe^{2+} concentration and crenarchaeol abundance are likely due to the strong correlation of Fe^{2+} with pH (Figure S5; Amenabar and Boyd, 2018), the true driver of crenarchaeol abundance. None of the individual environmental variables exhibited significant ($p < 0.05$) simple linear regressions with crenarchaeol abundance, but several combinations of variables exhibit significant multiple linear regression relationships with crenarchaeol (Table S3). Of all possible variable combinations (127 models), the most important environmental parameters for predicting crenarchaeol abundance were pH, SPC, and ORP. All five multiple linear regression models with the highest adjusted R^2 values include these three variables, which alone explain 19% of the variance (adj-R^2 = 0.19) (Table S4). The model that incorporates sulfide as a fourth variable in addition to pH, SPC, and ORP is the best overall predictor (adj-R^2 = 0.21). In contrast, including DO or temperature as the fourth variable decreases the model explanatory power (adj-R^2 = 0.17).

Spearman's rho tests of RI values showed that pH, ORP, and Fe^{2+} concentration were significantly associated with both the CL and IPL fractions from the YNP hot spring samples (Table S5). Only the CL fraction had a non-linear association with temperature. Simple linear regression results matched those of the Spearman's rho correlation, with pH, ORP, and Fe^{2+} concentration correlating with both CL and IPL fractions, while temperature only correlated with the CL fraction (Table S6). Notably, sulfide has a significant linear relationship with IPL-RI, but there is no non-linear association (Spearman's) between these two variables. Of all 127 possible multiple linear regression models of RI, the ten most significant ($p < 0.05$) models include pH and DO, while Fe^{2+} is present in eight, temperature in six, sulfide in five, SPC in three, and ORP in two (Table S7). The best explanatory models incorporate pH, temperature, DO, and Fe^{2+} (adj-R^2 = 0.80), or just the three variables pH, DO, and Fe^{2+} (adj-R^2 = 0.79). The addition of a fourth variable other than temperature slightly decreases model predictive power, but all ten most significant models exhibit an adjusted R^2 range of 0.79 to 0.80.

3.2 Comparison to previously published studies

We compiled published hot spring lipid samples (N = 299 including 41 from this study) that report pH, temperature, and iGDGT abundances, specifically including crenarchaeol abundance (Pearson et al., 2004; Zhang et al., 2006; Schouten et al., 2007; Pearson et al., 2008; Pitcher et al., 2009; Zhao et al., 2011; Burgess et al., 2012; He et al., 2012; Li et al., 2013; Boyd et al., 2013; Wu et al., 2013; Paraiso et al., 2013; Jia et al., 2014; Xie et al., 2015). We include relevant culture data in Figure 3 for context, but exclude this data from our statistical analyses to focus on environmental samples. For previous studies that split iGDGTs into CL and IPL fractions, the CL crenarchaeol relative abundances were used in this compilation since CL-iGDGTs are generally dominant and represent a more integrative record of iGDGT production than IPL lipids. The compiled dataset affords greater environmental context than the dataset from YNP samples alone; however, it reduces the available environmental variables to pH and temperature, which we focus on in our interpretation.

Across all sites, crenarchaeol abundances were highest to the alkaline side (≥ 7.0 pH) of the temperature-dependent neutral pH line (Equation 3), while acidic (< 7.0 pH) springs frequently have non-detectable levels of crenarchaeol (Figure 3). The 109 acidic samples have an average fractional crenarchaeol abundance of 0.02 (2% of all iGDGTs or CL iGDGTs), while that of the 190 alkaline samples is 0.10, with many examples > 0.50. Crenarchaeol was undetectable in 35/109 (32.1%) of acidic samples vs. 12/190 (6.3%) of alkaline samples. Crenarchaeol abundance also shows a weak relationship to temperature. Of 201 samples from environments ≥ 60 °C, 79.6% have detectable crenarchaeol. Ninety-eight samples are from < 60 °C, of which 93.9% contain detectable crenarchaeol. Additionally, at ≥ 60 °C, the average crenarchaeol fractional abundance is 0.04 (0.05 without zero values) and < 60 °C, the average is 0.14 (0.15 without zeroes).

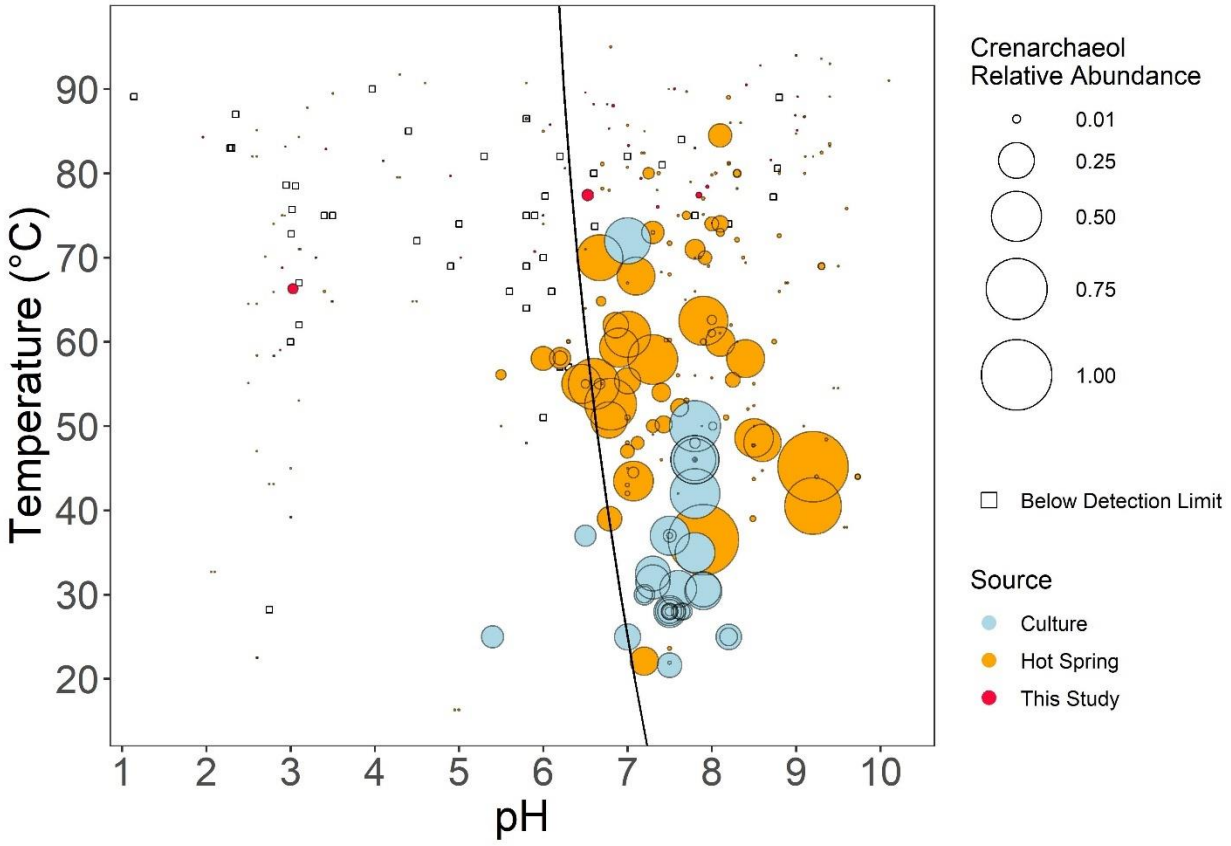

Figure 3. Relative abundances of crenarchaeol for all compiled hot spring samples (N = 299) and culture samples (N = 33). Samples with no detectable crenarchaeol are represented by squares and those with crenarchaeol present are circles filled by the source of the data. Area of circles correlates with crenarchaeol relative abundance. The black curve is the temperature-dependent neutral pH line (Equation 3).

3.3 Statistical analyses

Simple and multiple linear regression models were conducted to evaluate the influence of pH, temperature, and the combination of both variables for the full dataset (Table 1). MLR models incorporating interactions between temperature and pH and quadratic variables were run, but did not noticeably improve R^2 values (0.13 with interactions and 0.15 with quadratic variables for the crenarchaeol models), so linear models are shown for simplicity. Non-linear Spearman's rho correlations indicated that crenarchaeol is strongly associated with both pH and temperature ($p = 1 \times 10^{-13}$ and 5×10^{-9}, respectively), while Ring Index (Equation 1) is associated with pH ($p = 7 \times 10^{-9}$) but not with temperature ($p = 0.8$). While all R^2 values show relatively low explanatory power, pH dominates predictions of RI, while both pH and temperature are significant individual predictors of crenarchaeol abundance.

Table 1. Outputs of simple and multiple linear regression models for pH and temperature relationships with crenarchaeol abundance and Ring Index of all compiled data (N = 299). Adjusted R^2 values are reported, and significant p-values are indicated by bold italics. Note that negative R^2 values indicate a fit worse than a horizontal line.

		Crenarchaeol		**RI**	
	Parameter(s)	**p-value**	**adjusted R^2**	**p-value**	**adjusted R^2**
Simple Linear Regression	pH	**<0.001**	0.033	**<0.0001**	0.15
	Temp (°C)	**<0.0001**	0.073	0.62	-0.0025
Multiple Linear Regression	pH + Temp (°C)	**<0.0001**	0.11	**<0.0001**	0.15

The two variables are visualized in Figure 4. Relative crenarchaeol abundance is lower in many high-temperature samples and lower or absent in most of the lowest-pH samples (Figures 4A, 4B). RI has no apparent patterns associated with temperature, but low RI values are clearly disfavored in low-pH samples (Figures 4C, 4D). While the linear regression models are statistically significant, all these correlations are modest (Table 1), and some of the highest RI values occur at high pH values (e.g., Figure 4C).

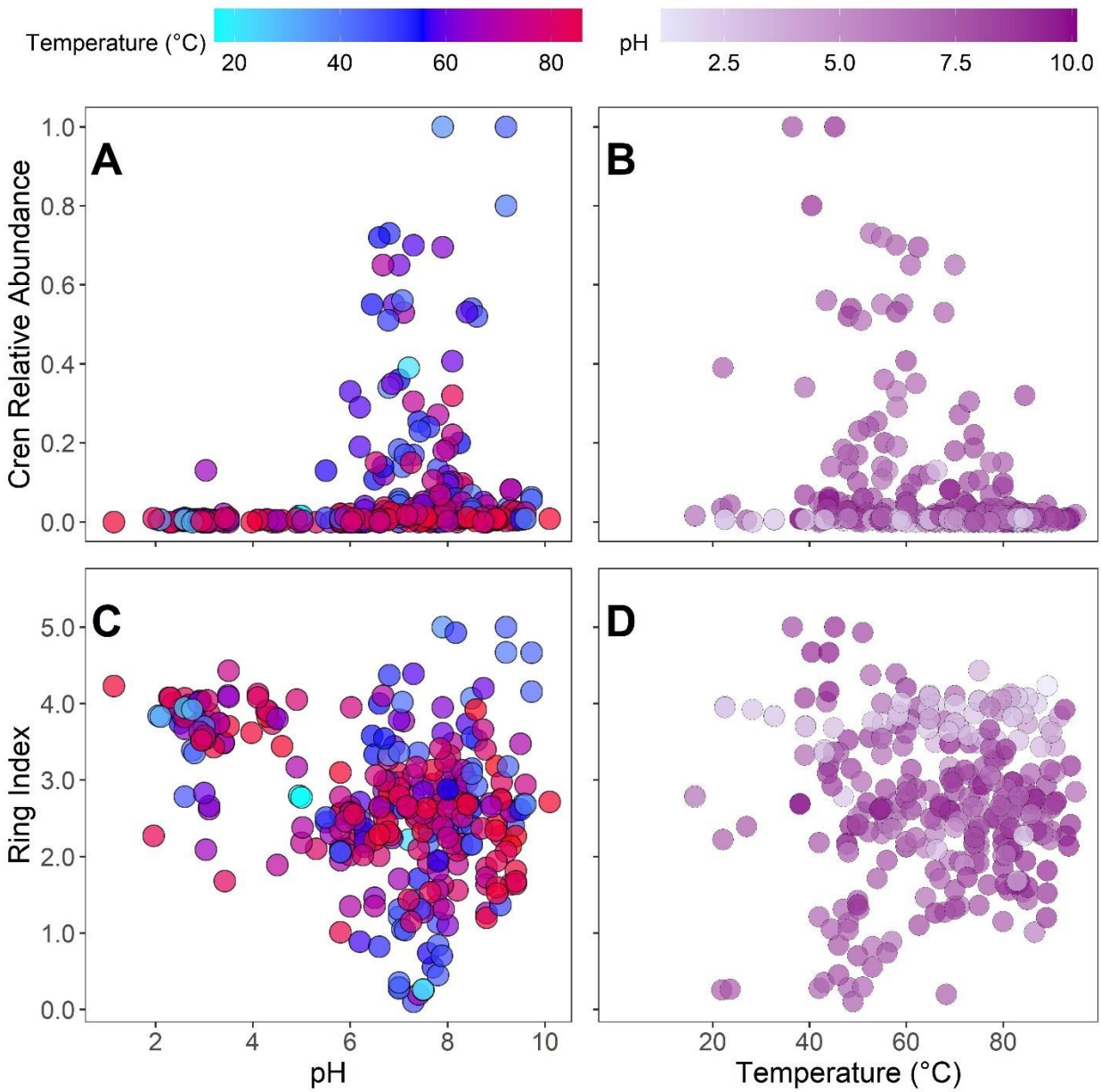

Figure 4. Crenarchaeol relative abundance versus (A) pH and (B) temperature for the 299 compiled samples, with fill by the other variable. Ring Index versus (C) pH and (D) temperature for the 299 compiled samples, with fill by the other variable.

4. Discussion

4.1 Environmental Predictors of Ring Index

Studies of marine systems generally consider temperature to be the primary driver for iGDGT cyclization (Schouten et al., 2002; Kim et al., 2008; Kim et al., 2010; Tierney, 2012), which may result from the relative geochemical uniformity of modern open-ocean environments. In marine waters, deviations from global average RI or TEX_{86} vs. temperature correlations are associated with anomalous water chemistry, including DO, pH, and other carbon system parameters (Qin et al., 2015; Hurley et al., 2018; Elling et al., 2015; Hurley et al., 2016), demonstrating that variables other than temperature may be of greater importance in other settings (Elling et al., 2015; Boyd et al., 2011; Cobban et al., 2020). It is likely that control of iGDGT cyclization in hot springs is different from the marine system, because hot springs generally span larger environmental gradients, including but not limited to pH. Previous studies examining iGDGT cyclization in hot springs have yielded conflicting conclusions. Temperature, pH, salinity, redox balance, bicarbonate concentration, growth rate, and DO all have been reported to correlate with iGDGT cyclization (Elling et al., 2015; Zhou et al., 2020; Evans et al., 2018, Pearson et al., 2004; Boyd et al., 2013; Cobban et al., 2020; Qin et al., 2015). While the degree of importance of each of these variables on iGDGT cyclization has not been definitively established, some studies conclude that pH has a greater influence than temperature. For example, hot springs spanning pH 5.5 to 7.2 in New Zealand showed increased RI at higher temperatures, but more acidic springs (pH 2.1 to 5.5) did not follow this trend (Kaur et al., 2015). These results indicate that acidity is more important than temperature for affecting archaeal membrane composition, potentially in direct response to pH-induced stress. The discrepancies among studies may be due to sampling relatively narrow ranges of geochemical and geophysical parameters, or it may result from the competing effects of several environmental factors (e.g., temperature and pH; Wu et al., 2013; Boyd et al., 2013; Pearson et al., 2008; Xie et al., 2015). We synthesize prior works and our new observations from Yellowstone to consider the environmental stressors of pH and temperature together, rather than in isolation.

Here, our analysis of compiled global hot springs (N = 299) demonstrates that pH significantly influences RI, while temperature does not. Linear regression models for the 41 YNP samples indicate that pH alone

287 predicts a majority of the RI distribution in hot springs (CL, 64%; IPL, 55%), consistent with previous hot
288 springs studies that concluded pH is the primary predictor of both RI (Pearson et al., 2008; Boyd et al.,
289 2013) and the distribution of genes related to cyclopentyl ring production (Blum et al., 2022). ORP
290 emerges as an important predictor of RI in linear regressions of the YNP dataset (CL = 31%; IPL = 31%),
291 consistent with earlier findings that redox conditions are important for archaeal lipid stress responses
292 (Cobban et al., 2020). Spearman's rho correlations and simple linear regression models highlight the
293 influence of ORP on membrane lipid cyclization. However, when considering redox conditions alongside
294 pH, dissolved oxygen (DO) emerges as a better supplementary variable for Yellowstone samples. DO and
295 ORP are closely related indicators of the oxidation state of hot spring environments, but ORP has a direct
296 relationship with pH, which likely contributes to its association and simple regression significance with
297 RI (James and Lytle, 2004). Consequently, DO is the more independent variable to assess the relationship
298 between redox stress and iGDGT cyclization. Following ORP (or DO), Fe^{2+} emerges as a potential control
299 on archaeal membrane dynamics (predictive power: CL, 22%; IPL, 22%). Free intracellular Fe^{2+} is known
300 to contribute to oxidative stress experienced by microbial cells through the Fenton reaction (Touati,
301 2000). However, the covariation of Fe^{2+} with decreasing pH makes it difficult to determine whether Fe^{2+}
302 has any independent effect (Figure S5). Sulfide concentration exhibits minimal predictive power, with
303 influence only on IPL-RI in a linear regression (11%), but not on CL-RI, nor any significant Spearman's
304 rho association. This pattern may indicate that any short-timescale influence of sulfide on iGDGT
305 cyclization is overpowered by other variables over longer time periods. Similarly, temperature is
306 associated with CL-RI but not IPL-RI, but this may be explained by differing CL and IPL crenarchaeol
307 abundances in one or two samples that drive the CL correlation over the significance threshold (see
308 Supplement for detailed discussion). It is also possible that temperature influences RI over long time
309 periods (CL), while other variables have greater control over ring abundances in extant communities
310 (IPL).
311
312 **4.2 Predictors of Crenarchaeol Abundance**

313 Crenarchaeol relative abundance, like RI, was associated with multiple environmental variables. While
314 pH, temperature, and redox explain the majority of the variance of RI (MLR: $R^2 = 0.80$), temperature and
315 pH are both only weakly associated with crenarchaeol abundance (SLR: Temp $R^2 = 0.07$, pH $R^2 = 0.03$)
316 and combining them adds minimal explanatory power (MLR: $R^2 = 0.11$; See Table 1). The variables
317 examined in this study do not sufficiently explain cyclohexyl ring distributions, and simple linear
318 regressions cannot determine the rank order of influence of pH and temperature on crenarchaeol
319 distributions. The relative importance of the two variables also is inconclusive for the non-linear
320 Spearman's rho tests. The clear tradeoff between statistical power (N = 299 and N = 41) and geochemical
321 detail (two variables versus seven) between the compiled and the Yellowstone-only datasets demonstrates
322 the need for consistent variable collection and robust analyses to evaluate a ranked list of variables
323 important for crenarchaeol production.
324
325 While temperature is associated with crenarchaeol abundance in the global hot spring dataset, it is not
326 associated with crenarchaeol abundance in the more geochemically detailed YNP dataset. The latter
327 observation may be attributed to a lower representation of samples below 60 °C for the YNP dataset (N =
328 2) compared to the global dataset (N = 96). This result suggests that temperature is associated with
329 crenarchaeol abundance, but that its relationship is weaker than that of pH. Variables present exclusively
330 in the Yellowstone dataset (e.g., ORP and DO) covary with temperature and may contain a temperature
331 signal. An early examination of crenarchaeol from hot springs found that bicarbonate concentration, not
332 temperature, correlated with crenarchaeol distribution (Pearson et al., 2004). While that study included
333 pH, samples were limited to six regional springs that spanned pH values of 6.4 to 9.2, a range that would
334 not show the pH signal observed in our current study.
335
336 The strong association between pH and crenarchaeol abundance is perhaps unsurprising. Without
337 protective adaptations to external pH, a cell's pH homeostasis can be disrupted, thus slowing enzyme
338 activity, destabilizing other proteins and nucleic acids, and potentially resulting in cell death (Slonczewski
339 et al., 2009). Crenarchaeol is ubiquitous in marine environments and most literature on iGDGT

distributions is focused on marine paleoclimate applications, explaining why the influence of pH on crenarchaeol has remained uncharacterized. The average pH of Earths' surface oceans is 8.07 ± 0.02 between 60° North and 60° South (Jiang et al., 2019), but Thaumarchaeota also thrive in less alkaline marine thermoclines (pH 7.5 to 7.2 from 200 to 600 m depth; Church et al., 2010; Clayton and Byrne 1993; Palmer et al., 1998). The even larger pH range of terrestrial hot springs (1.14 to 10.10) covered in this compilation shows that crenarchaeol is present over a wide range of pH values (1.96 to 10.1), but is most relatively abundant (> 30% of core/total iGDGTs) from pH 6.0 to 9.2. While a pH range from 6.0 to 9.2 is relatively narrow for hot springs, it is much wider than that of the modern surface ocean (8.0 to 8.25; Jiang et al., 2019).

Differences in parameters (other than pH) that contribute to multiple linear regression models of crenarchaeol and RI indicate nuanced or independent processes influence production of cyclohexyl rings in iGDGTs. In addition to pH, important predictors of Ring Index are DO and Fe^{2+}, while those of crenarchaeol abundance are SPC, ORP, and temperature. While these secondary variables impact RI and crenarchaeol abundance differently, they can all potentially cause membrane stress related to redox conditions and/or ion concentrations, i.e., factors affecting transmembrane processes that help maintain cellular energy balance (Cobban et al., 2020; Zhou et al., 2020). It is possible that cyclohexyl rings have a specific relationship to cellular redox conditions, but this has not yet been shown conclusively. Growth rate correlates with GDGT cyclization in laboratory studies, indicating responsiveness to cellular energy availability (Cobban et al., 2020).

4.3 Temperature and pH Optima for Crenarchaeol Production

To test the hypothesis that the evolution of crenarchaeol in extremophilic archaea enabled them to invade moderate environmental niches, the optimal pH and temperature for crenarchaeol relative abundance were calculated (total data, N = 299; Figure 5). The pH bin with the highest mean crenarchaeol abundance is 7 to 7.5 while bins from pH values of 6.5 to 8.5 also have high sample counts with elevated means and upper quartiles relative to those outside of this pH range (Figure 5A). The bin from pH 9.5 to 10 also has

high crenarchaeol abundance (0.01 to 0.06), but this may be an artifact of the small site number (N = 5), demonstrating the need for further quantification of archaeal lipids in alkaline springs. The temperature bin with the highest mean crenarchaeol abundance spans 50 to 55 °C, while bins from 40 to 60 °C have elevated mean and upper quartile values relative to those outside this range (Figure 5B). In general, bins from 40 to 90 °C have high sample counts while bins from 15 to 40 °C and above 90 °C have low sample counts, explaining the high upper quartile value of the bin from 35 to 40 °C (N = 7).

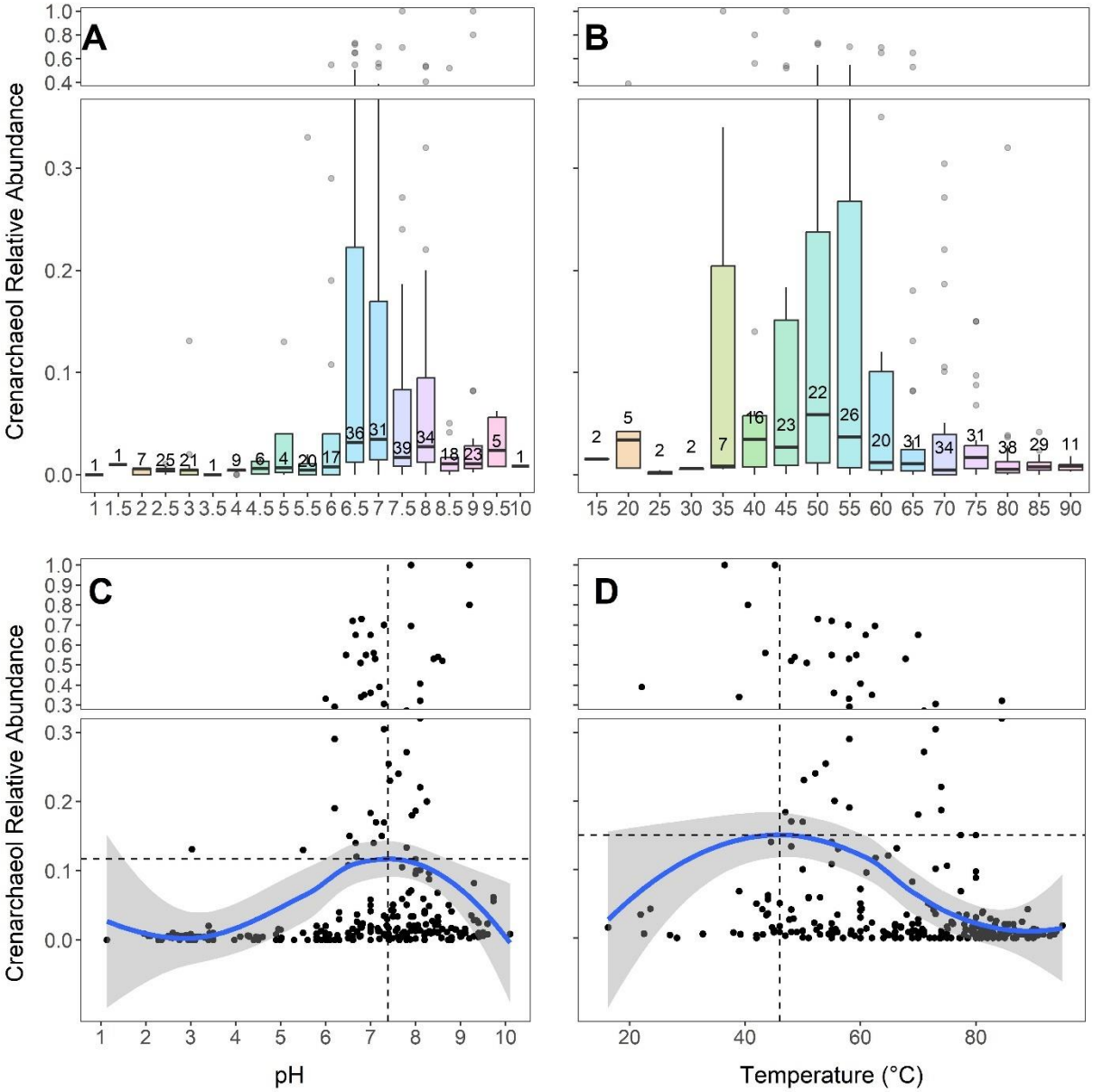

Figure 5: Boxplots (A &B) and LOESS smoothing curves (C&D) of crenarchaeol relative abundances of compiled data (N = 299). Data are binned by 0.5 pH units (A) and 5 °C temperature units (B) with bins labelled by their minimum bound. Median and quartile abundances are visualized in boxes and maximum and minimum values are indicated by whiskers. Sample counts for each bin are included above mean value indicators in A and B. The functions plotted in C and D have 95% confidence intervals shaded in gray. Dashed lines in C and D represent x and y values where crenarchaeol reaches its maximum. Y-axis breaks and scale changes are utilized to allow outliers to be visualized.

373

The LOESS (locally weighted smoothing; Figures 5C and 5D) functions show the optimal pH for crenarchaeol is 7.4 (corresponding to 0.12 LOESS-predicted relative abundance), consistent with the boxplot having the highest mean (pH 7 to 7.5) in Panel 5A. The optimal temperature for crenarchaeol is 46 °C, (0.15 LOESS-predicted relative abundance). While this value is not within the highest-mean bin of Panel 5B (50 to 55 °C), it does fall within the broad grouping of temperatures showing elevated mean crenarchaeol abundances (40 to 60 °C); this is consistent with temperature having a weaker overall control on iGDGT, and specifically crenarchaeol, patterns compared to pH. Scatter in Panel 5D shows that crenarchaeol can also be found in high abundances above 80 °C. Hot spring data are expected to have some degree of noise due to environmental variability over several timescales including changes in volcanic/hydrothermal activity, seasonality, and diurnal cycles (Colman et al., 2021; see Supplement for further discussion).

The analysis shown in Figure 5 corroborates the observed circumneutral pH threshold identified in Figure 3, in which instances of abundant crenarchaeol track the temperature-dependent neutral pH line. The directionality of the relationship of crenarchaeol with environmental parameters supports the hypothesis that crenarchaeol acts to expand archaeal membranes (in opposition to cyclopentyl rings), enabling adaptations of thermophilic/acidophilic archaea to less extreme environments, such as soils and oceans of moderate temperature and pH (Schouten et al., 2000). Acidic environments have an excess of protons, promoting the need for cell membrane compaction through cyclopentyl ring production to prevent energetic imbalances. If crenarchaeol expands membrane fluidity, crenarchaeol concentrations should be expected to be lower in acidic environments. While there exists an abrupt acidity cutoff for high relative crenarchaeol production, there is no apparent upper pH limit (Figure 3). This may indicate that high pH is not as stressful as acidic pH for archaeal cells. Nevertheless, further study of alkaline environments from pH 9 to 12 could illuminate a decrease in crenarchaeol production if an excess of hydroxyl ions poses significant stress to archaeal cells.

4.4 Integrating Lipid Data with Geochemistry and Metagenomics

401 *Increased contextualization of lipid abundance measurements*

402 Given the association of crenarchaeol abundance with multiple environmental parameters identified in
403 this study, comprehensive analyses that quantify the relative influence of environmental variables on
404 crenarchaeol abundance will help guide interpretations of this biomarker in the sediment record. Our
405 results indicate that pH may be the environmental variable with the most influence on both crenarchaeol
406 abundance and RI distributions, and therefore pH may have the greatest control on overall archaeal
407 membrane dynamics. Nevertheless, further research, such as independent manipulations of variables in
408 culture, will strengthen this conclusion. Future studies investigating iGDGT cyclization should collect a
409 standardized suite of environmental parameters to tease apart the relative influence of multiple factors.
410 Every entry in our global hot spring compilation contains temperature and pH measurements, but other
411 parameters, such as ORP, SPC, DO, and various dissolved ions, are important targets that are notably
412 lacking.

413

414 *Coordination of metagenomic and transcriptomic studies with lipid analyses*

415 The understanding of archaeal cyclopentyl ring synthesis was revolutionized by the discovery of *grsAB*
416 (Zeng et al., 2019), but the gene(s) encoding cyclohexyl ring formation remain elusive. The relatively
417 large body of data now available from both terrestrial and marine settings indicates that candidate
418 organisms for genomic studies should be targeted in circumneutral and mesophilic settings. To test the
419 long-standing belief that crenarchaeol is specific to Nitrososphaerota (Pearson and Ingalls, 2013;
420 Schouten et al., 2013), correlating the abundance of crenarchaeol with different taxonomic groups could
421 either support or contradict this assertion (Sinninghe-Damsté et al., 2018). In addition, to identify genes
422 related to cyclohexyl ring production, transcriptomic studies should evaluate gene expression in concert
423 with high and low crenarchaeol abundances. Laboratory experiments aiming to produce abundant
424 crenarchaeol from enrichment cultures will benefit from targeting temperatures from 40 to 55 °C and pH
425 values from 6.5 to 8.0 (Figures 5A, 5B), while pairing with comparative transcriptomics or proteomics
426 data to identify the cyclohexyl ring biosynthesis enzyme.

427

4.5 Implications for the History of Crenarchaeol

If Nitrososphaerota evolved from thermophilic hot spring ancestors that produced membranes with high cyclopentyl ring abundances to protect against extremes in pH and temperature, these organisms would have required a mechanism to increase membrane fluidity to transition to cooler and more alkaline marine waters. This study supports the mesophilic and circumneutral favorability of crenarchaeol as a key adaptive molecule, in agreement with the hypothesis that crenarchaeol expands lipid membranes to afford greater cellular membrane flexibility. Given our larger range of environmental variables and higher sampling density than previous studies, the temperature optimum of crenarchaeol from this study (46 °C) is likely representative, while the prior estimated optimum of 40 °C (Zhang et al., 2006) is within the elevated range of the 95% confidence interval of the model (Figure 5). It also agrees with sea-surface temperature reconstructions during significant evolutionary events associated with the radiation of crenarchaeol-producing AOA. The predicted dates of the transition of AOA into the ocean (1017 Ma, Ren et al., 2019; 509 Ma, Yang et al., 2021) correspond to an estimated ocean temperature range between 30 and 65 °C (Mesoproterozoic: 1600 to 1000 Ma; Robert and Chaussidon, 2006) or a mean low-latitude estimate of 47 °C (Cambrian Period: 541 to 485 Ma; Grossman and Joachimski, 2022), which is significantly warmer than modern oceans. Moreover, the proposed expansion of non-thermophilic marine Nitrososphaerota during the mid-Cretaceous anoxic event (ca. 112 Ma) may have occurred in comparatively warm marine settings of 33 to 42 °C (Bice et al., 2006). Precise constraints on the timing and rate of archaeal evolution will come from a more detailed understanding of archaeal lipid synthesis in extant organisms as they are cultivated and characterization of lipid production and modification mechanisms in environmental boundary conditions.

5. Acknowledgements

This work was supported by a Dartmouth Stamps Scholarship (ANC), the Walter and Constance Burke Award of Dartmouth College (WDL), an NSF-EAR grant (WDL), NASA grant 80NSSC19M0150 (DRC and ESB), and an ACS-PRF award (AP). We thank C. Hendrix, S. Gunther, and A. Carlson at Yellowstone National Park for permitting research access under YNP permit #5544. We also wish to thank M. Palucis (Dartmouth) for help with the design of the Yellowstone map. We thank D. Payne (MSU), L. Denoncourt (MSU), and John Spear (Colorado School of Mines) for field assistance.

SUPPLEMENTAL INFORMATION

FIGURES

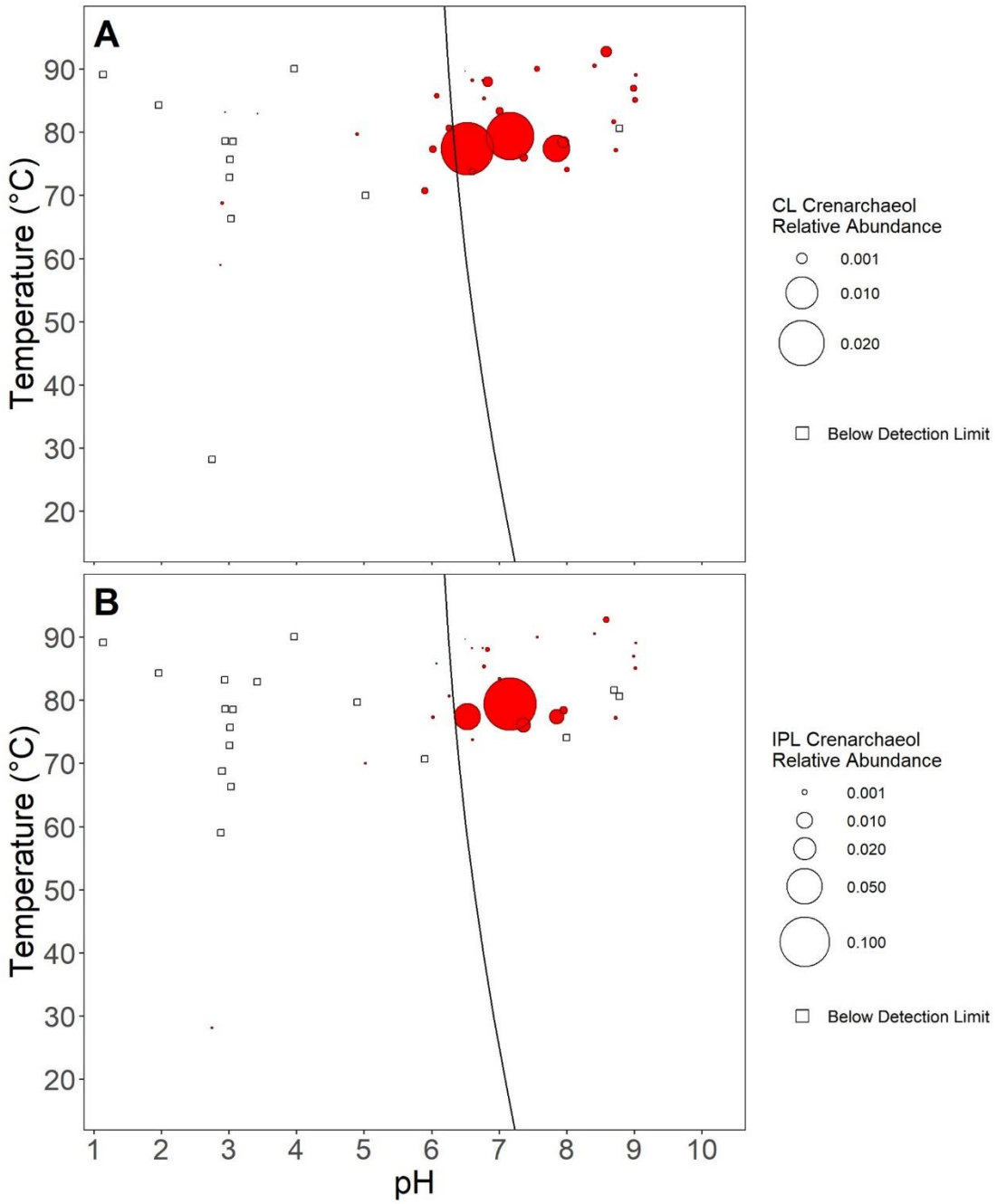

Figure S1. Relative abundances of (A) CL and (B) IPL crenarchaeol in temperature-pH space for 41 Yellowstone field samples collected from 2018-2022. Bubble area is proportional to relative abundance of crenarchaeol while squares represent non-detectable abundances. The black curve is the temperature-dependent neutral pH line (Equation 3).

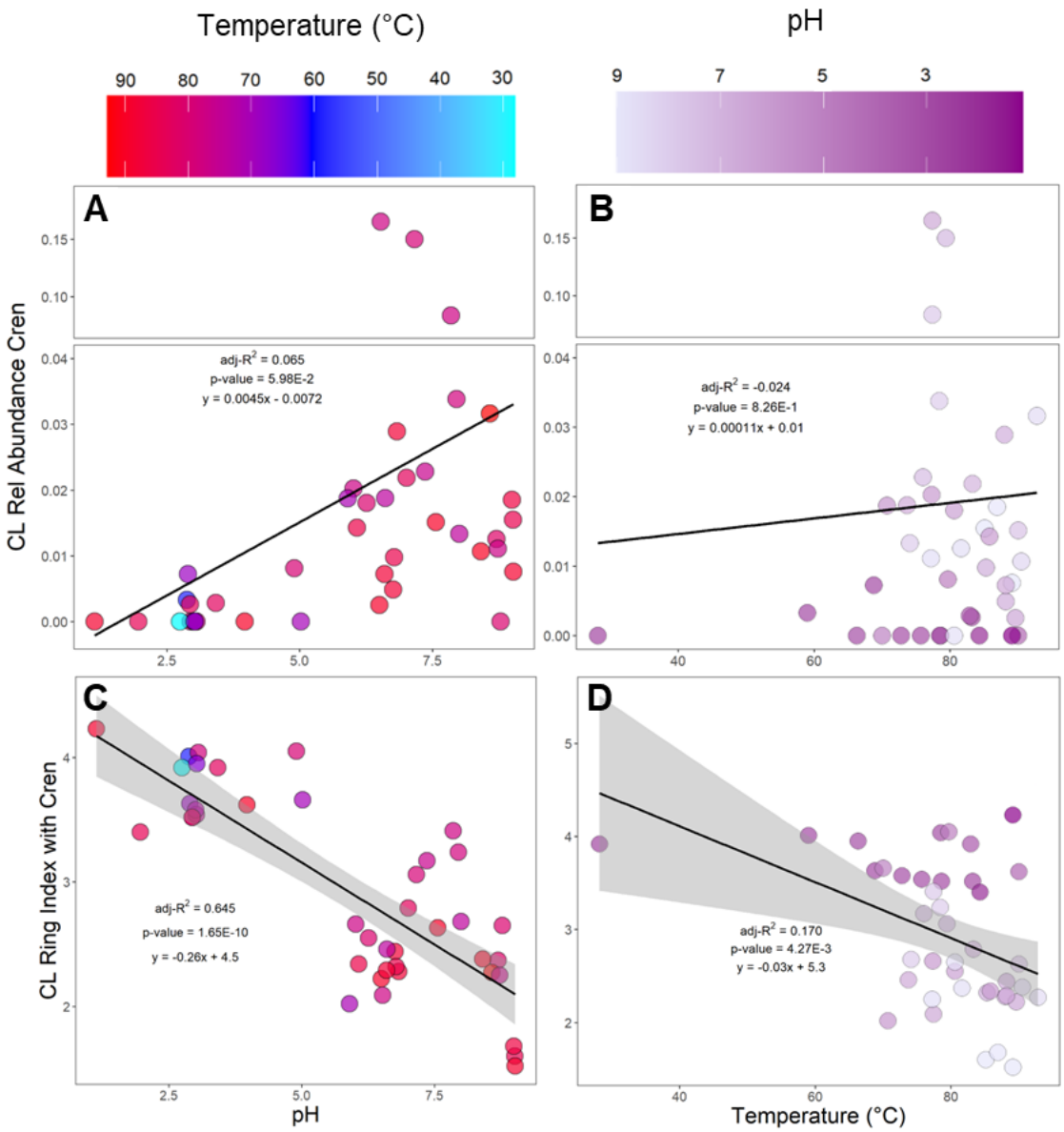

Figure S2. Relative abundances of CL crenarchaeol versus (A) pH and (B) temperature and Ring Index (with cren) versus (C) pH and (D) temperature for Yellowstone samples (N = 41) with fill by the other variable. Equations of lines of best fit, p-values, and adjusted-R^2 values are included. A y-axis break and scale change are utilized to include high abundance outliers of crenarchaeol abundance while visualizing detailed distributions of the majority of samples. Significant RI linear relationships have 95% confidence intervals shaded in gray.

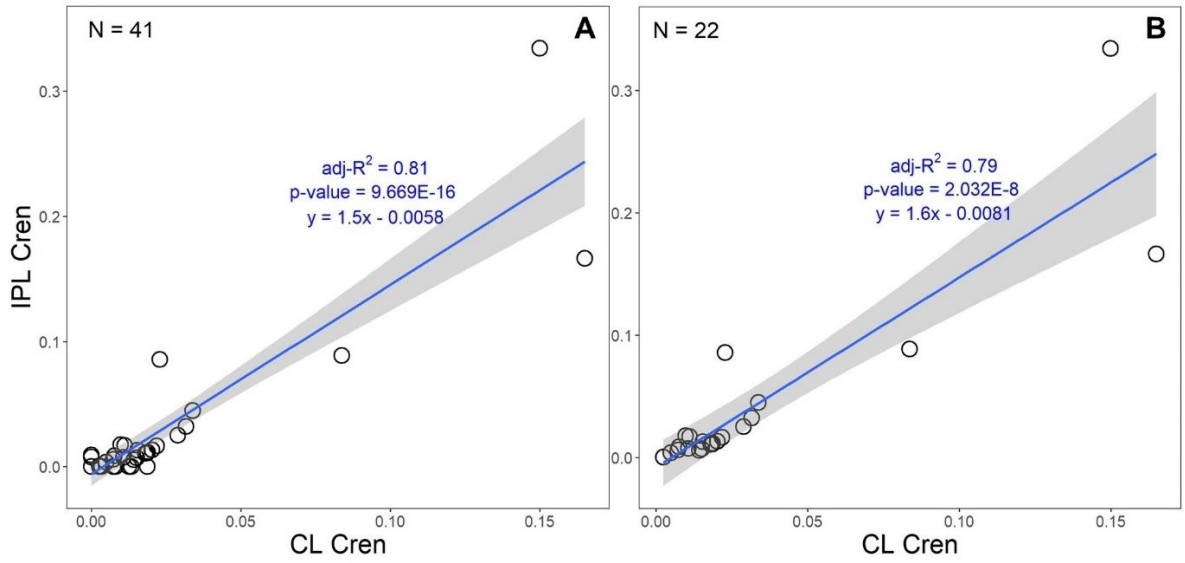

Figure S3. Linear regression model of IPL versus CL crenarchaeol relative abundance for each Yellowstone site. Panel (A) includes all sites while panel (B) excludes sites with zero values for CL or IPL crenarchaeol. The 95% confidence interval is shaded in gray and summary statistics are included.

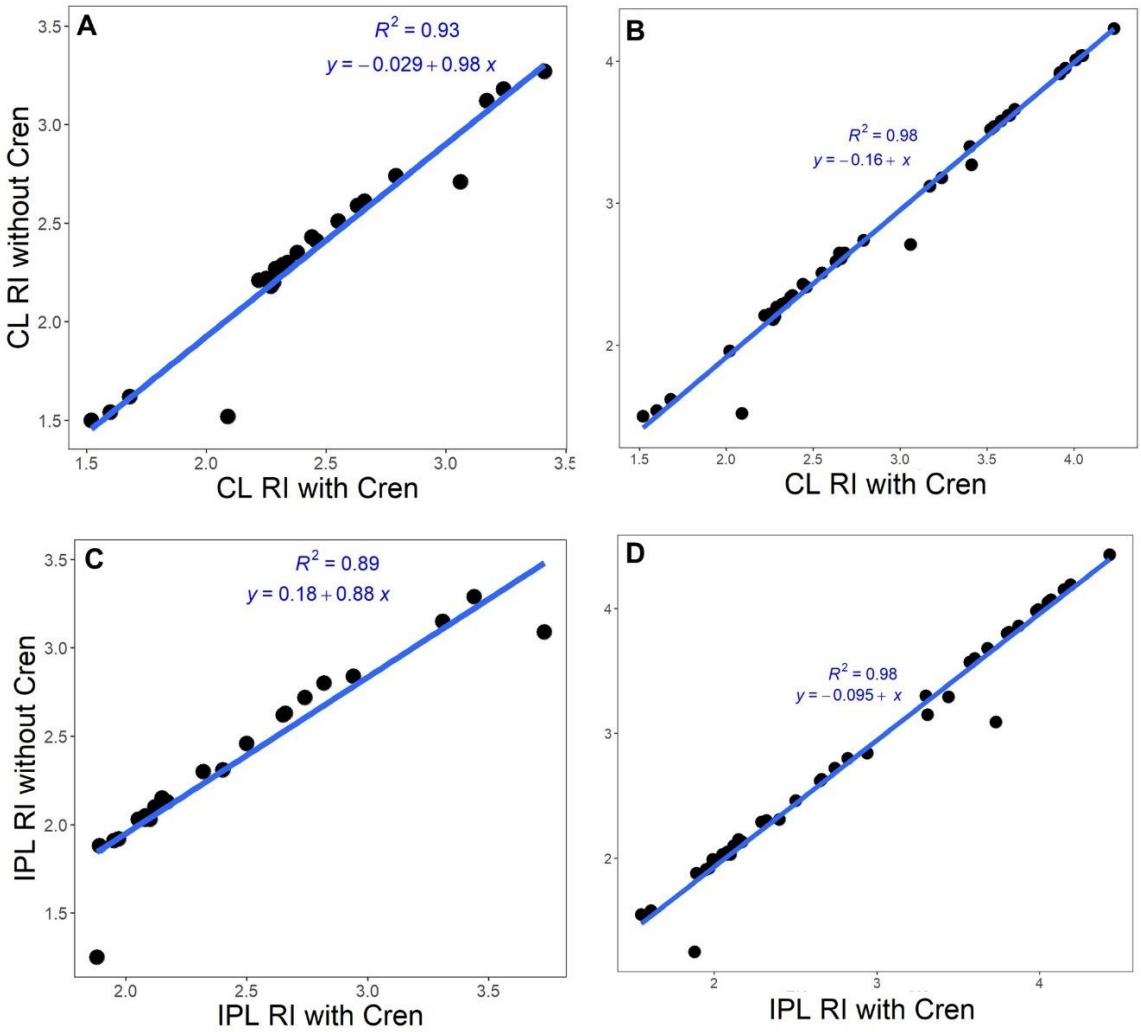

Figure S4. Simple linear regressions between Ring Index calculated without and with crenarchaeol for CL and IPL GDGT fractions from Yellowstone samples (See Equations 1 and 2). Panels (A) and (B) represent hot springs with detectable amounts of crenarchaeol (N = 30), while Panels (C) and (D) have values from all 41 hot spring samples regardless of crenarchaeol presence.

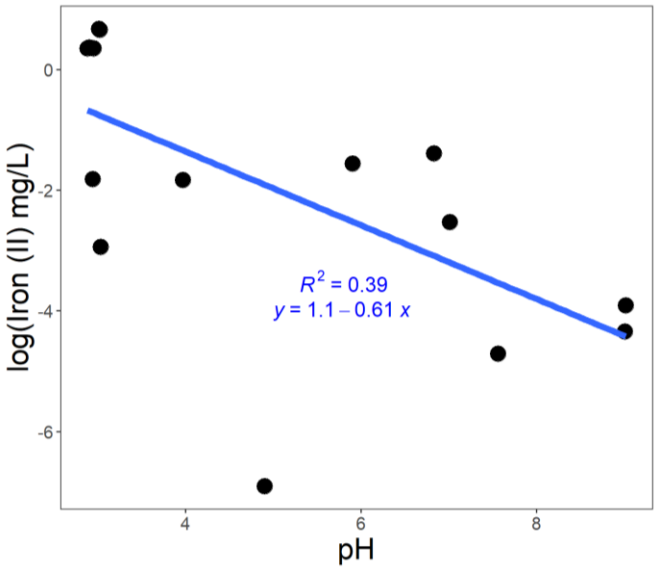

Figure S5. Simple linear regression of the log of Fe^{2+} concentration with pH for hot springs with data for both parameters (N = 31). Non-finite log values are excluded, and the Spearman's rho correlation p-value is 9.73×10^{-5}.

SUPPLEMENTAL TABLES

Yellowstone Crenarchaeol

Table S1. Field geochemical and geophysical parameters, crenarchaeol abundances, and ring indices for 41 samples from Yellowstone National Park collected during field seasons from 2018-2022.

Site Name	Year Sampled	Latitude (decimal degrees)	Longitude (decimal degrees)	pH	Temperature (°C)	Specific Conductivity (µS/cm)	Oxidation Reduction Potential (mV)	Dissolved Oxygen (mg/L)	Fe^{2+} (mg/L)	S^{2-} (µg/L)	CL Cren	CL Cren'	CL Cren+Cren'	CL RI With Cren	CL RI Without Cren	IPL Cren	IPL Cren'	IPL Cren+Cren'	IPL RI With Cren	IPL RI Without Cren
Perpetual Spouter	2018	44.7265959	-110.709133	7.01	83.3	2792	-123	0.81	0.08	10	0.019	0.0025	0.022	2.79	2.74	0.015	0.0017	0.016	2.50	2.46
Beowulf Main	2018	44.7314663	-110.711362	2.95	78.6	2117	-102	0.12	1.42	1580	BDL	BDL	BDL	3.52	3.52	BDL	BDL	BDL	3.99	3.99
Beowulf Upper	2018	44.7316004	-110.711316	2.90	68.8	2130	-39	0.70	1.44	470	0.0072	BDL	0.0072	3.63	3.62	BDL	BDL	BDL	3.99	3.99
Beowulf Orange	2018	44.7315187	-110.711363	2.88	59.0	2165	207	1.99	1.42	170	0.0033	BDL	0.0033	4.01	4.01	BDL	BDL	BDL	3.30	3.30
Dragon Left Source	2018	44.7318275	-110.711154	3.02	75.7	2040	-90	0.21	1.94	1080	BDL	BDL	BDL	3.54	3.54	BDL	BDL	BDL	3.80	3.80
Dragon Stage Right Pool	2018	44.7318232	-110.71092	3.01	72.8	2018	-94	0.55	1.97	600	BDL	BDL	BDL	3.58	3.58	BDL	BDL	BDL	3.57	3.57
Hot South Dragon Detached	2018	44.7317765	-110.710901	3.06	78.5	1930	-129	0.09	NA	NA	BDL	BDL	BDL	4.04	4.04	BDL	BDL	BDL	4.05	4.05
Cold Sulfur Pool	2018	44.7318089	-110.711018	2.75	28.2	2489	159	0.45	NA	NA	BDL	BDL	BDL	3.92	3.92	0.0026	0.0052	0.0078	3.87	3.86
Cinder Pool (East Edge)	2018	44.7324835	-110.709773	3.97	90.0	2500	-215	0.19	0.16	430	BDL	BDL	BDL	3.62	3.62	BDL	BDL	BDL	3.98	3.98
Rabbit Creek Source Pool #1	2018	44.5211885	-110.811781	9.01	85.1	2042	-315	0.47	0.01	10	0.0078	0.0077	0.015	1.60	1.54	0.0037	0.0093	0.013	2.17	2.13
Rabbit Creek Source Pool #2	2018	44.5198758	-110.810763	9.02	89.1	2119	-332	0.60	0.02	1290	0.0052	0.0024	0.0076	1.52	1.50	0.0023	0.0062	0.0086	2.32	2.30
Sour Rabbit	2018	44.519861	-110.810686	4.90	79.7	140	-56	1.13	0.00	0	0.0081	BDL	0.0081	4.05	4.04	BDL	BDL	BDL	3.81	3.81
Scaffold	2018	44.5190822	-110.809149	8.70	81.6	1760	-130	0.79	0.00	0	0.011	0.0011	0.013	2.37	2.34	BDL	BDL	BDL	1.99	1.99
Roadside Rabbit Creek	2018	44.51719	-110.822738	7.56	90.0	1852	-272	0.41	0.01	40	0.013	0.0017	0.015	2.63	2.59	0.0072	BDL	0.0072	2.82	2.80
Beryl Spring	2019	44.6787113	-110.746493	6.76	88.2	2514	-255	0.48	0.00	153	0.0049	BDL	0.0049	2.44	2.43	0.0026	0.0011	0.0036	1.89	1.88
Bijah Spring	2019	44.7611	-110.73097	7.36	76.0	1470	-25	1.63	0.00	27	0.021	0.0022	0.023	3.17	3.12	0.078	0.0080	0.086	3.44	3.29
Yuppie Sulfur	2019	44.72041	-110.71326	2.94	83.2	1182	267	0.29	0.16	17	0.0026	BDL	0.0026	3.52	3.52	BDL	BDL	BDL	3.68	3.68
Gassy Gibbon	2019	44.68406	-110.74355	6.83	88.0	48	-238	0.51	0.25	87	0.024	0.0053	0.029	2.28	2.20	0.014	0.011	0.025	2.10	2.03
Acid Bridge	2019	44.73616	-110.70644	1.14	89.1	4473	311	0.22	NA	213	BDL	BDL	BDL	4.23	4.23	BDL	BDL	BDL	4.43	4.43
Driveway Spring (No Parking)	2022	44.4626324	-110.852994	7.95	78.4	2200	-102	1.09	0.00	0	0.034	BDL	0.034	3.24	3.18	0.041	0.0043	0.045	2.94	2.84
Pentagonal Spring (SOB)	2022	44.463439	-110.852837	7.85	77.4	2234	-124	1.95	0.00	0	0.068	0.016	0.084	3.41	3.27	0.089	BDL	0.089	3.31	3.15
Beryl Runoff	2022	44.6786827	-110.746465	6.78	85.3	2518	-288	0.67	NA	NA	0.0058	0.0041	0.010	2.32	2.29	0.0070	0.011	0.018	1.97	1.92
Beryl Main Overhang	2022	44.6786622	-110.746512	6.50	89.6	2513	-334	0.41	NA	NA	0.0025	BDL	0.0025	2.22	2.21	0.0003	BDL	0.0003	2.15	2.15
Beryl Side	2022	44.6787151	-110.746526	6.60	88.2	2525	-310	0.47	NA	NA	0.0051	0.0022	0.0072	2.29	2.27	0.0009	0.0050	0.0059	2.12	2.10
Splash Mountain	2020	44.69032	-110.72993	1.96	84.3	3409	331	0.39	NA	47	BDL	BDL	BDL	3.40	3.40	BDL	BDL	BDL	4.19	4.19
Corner Thing	2020	44.69067	-110.72977	6.08	85.8	5380	3	0.01	BDL	515	0.0087	0.0056	0.014	2.34	2.30	0.0016	0.0040	0.0056	2.05	2.03
Black Hole Sun	2020	44.69038	-110.7289	6.02	77.3	5090	54	0.16	BDL	73	0.017	0.0035	0.020	2.66	2.61	0.0094	0.0038	0.013	1.95	1.91
Angel Hair	2020	44.7536	-110.40418	6.53	77.4	1998	30	0.07	NA	2500	0.13	0.034	0.17	2.09	1.52	0.12	0.049	0.17	1.88	1.25
Bone Pool	2020	44.68915	-110.7285	6.61	73.7	5180	20	0.84	BDL	16	0.013	0.0057	0.019	2.46	2.41	0.0087	0.0027	0.011	2.65	2.62
Spitting Croissant	2020	44.69033	-110.72935	3.42	82.9	2465	237	0.15	NA	150	0.0029	BDL	0.0029	3.92	3.91	BDL	BDL	BDL	4.15	4.15
Citronella	2020	44.75154	-110.4151	8.00	74.1	4107	-68	1.02	BDL	2570	0.012	0.0014	0.013	2.68	2.65	BDL	BDL	BDL	1.55	1.55
Obsidian	2019	44.61006	-110.43882	5.90	70.7	1121	91	NA	0.21	130	0.0069	0.012	0.019	2.02	1.96	BDL	BDL	BDL	3.60	3.60
Bubbling Blonde	2019	44.73616	-110.70649	5.02	70.0	3635	NA	0.05	NA	7858	BDL	BDL	BDL	3.66	3.66	0.0019	0.0072	0.0092	1.61	1.58
Boulder Spring	2019	44.55878	-110.844	8.41	90.5	4040	-99	0.03	BDL	2190	0.0030	0.0077	0.011	2.38	2.35	0.0018	0.0055	0.0073	2.74	2.72
River (Broken Dreams)	2019	44.56153	-110.83685	6.26	80.6	3702	51	0.01	BDL	319	0.0078	0.010	0.018	2.55	2.51	0.0036	0.0070	0.011	2.66	2.63
The Hammer	2019	44.51987	-110.81077	8.99	86.9	4369	-132	0.33	BDL	1190	0.0096	0.0089	0.019	1.68	1.62	0.0039	0.0071	0.011	2.08	2.05
Mound Spring	2019	44.56485	-110.86005	8.58	92.8	3830	-111	0.01	BDL	1092	0.0095	0.022	0.032	2.27	2.18	BDL	0.032	0.032	2.40	2.31
Figure 8	2019	44.60993	-110.43939	3.03	66.3	4124	256	NA	0.05	13	BDL	BDL	BDL	3.95	3.95	BDL	BDL	BDL	4.07	4.07
Scaffold (Rabbit's Nest)	2019	44.51914	-110.80914	8.78	80.6	3602	-115	1.15	BDL	23	BDL	BDL	BDL	2.65	2.65	BDL	BDL	BDL	2.29	2.29
Mom's Spaghetti	2019	44.50889	-110.80895	7.16	79.4	905	-3	1.01	BDL	BDL	0.15	BDL	0.15	3.06	2.71	0.30	0.036	0.33	3.73	3.09
Azure Pool	2019	44.56097	-110.83286	8.73	77.2	3447	-117	0.83	BDL	345	0.0018	0.0093	0.011	2.25	2.22	BDL	0.017	0.017	2.08	2.03

Table S2 Spearman's rho correlation p-values for environmental parameters and crenarchaeol relative abundance from Yellowstone samples. Analyses are run for both core (CL) and intact polar lipid (IPL) fractions and significant correlations are indicated in bold italics.

	Cren Abundance	
Parameter	**CL**	**IPL**
pH	***<0.0001***	***<0.001***
Temp (°C)	0.63	0.49
DO (mg/L)	0.19	0.52
SPC (µS/cm)	0.54	0.77
ORP (mV)	0.47	0.10
Fe^{2+} (mg/L)	***0.0035***	***0.0025***
S^{2-} (µg/L)	0.10	0.42

Table S3: Outputs of simple linear regression models for environmental parameters and CL and IPL relative abundance of crenarchaeol from Yellowstone samples. The significance threshold is set to a p-value of 0.05 and any significant correlations would be indicated in bold italics.

	Crenarchaeol Abundance			
	CL		**IPL**	
Parameter	**p-value**	**adjusted R^2**	**p-value**	**adjusted R^2**
pH	0.06	0.07	0.15	0.03
Temp (°C)	0.83	-0.02	0.98	-0.03
DO (mg/L)	0.34	0.00	0.17	0.03
SPC (µS/cm)	0.18	0.02	0.09	0.05
ORP (mV)	0.99	-0.03	0.91	-0.03
Fe^{2+} (mg/L)	0.14	0.04	0.32	0.00
S^{2-} (µg/L)	0.91	-0.03	0.92	-0.03

Table S4. Outputs of 10 multiple linear regression models with highest adjusted R^2 values for environmental parameters and relative abundances of CL crenarchaeol from Yellowstone samples. The significance threshold is set to 0.05 and significant p-values are indicated in bold italics. Models are reported in order of decreasing adjusted R^2 values.

	Crenarchaeol Abundance		
Input Parameters	**p-value**	**Multiple R^2**	**Adjusted R^2**
pH, SPC, ORP, S^{2-}	***0.023***	0.31	0.21
pH, SPC, ORP, DO, S^{2-}	0.051	0.32	0.20
pH, Temp, SPC, ORP, S^{2-}	***0.048***	0.31	0.19
pH, SPC, ORP	***0.015***	0.25	0.19
pH, SPC, ORP, DO	***0.028***	0.27	0.19
, Temp, SPC, ORP, DO, S^{2-}	0.077	0.34	0.18
pH, Temp, SPC, ORP	***0.035***	0.25	0.17
pH, Temp, SPC, ORP, DO	0.056	0.28	0.16
pH, SPC, ORP, Fe^{2+}	0.12	0.24	0.12
DO, Fe^{2+}	0.086	0.17	0.11

Yellowstone Ring Index

Table S5. Spearman's rho correlation p-values for environmental parameters and Ring Index from Yellowstone samples. Analyses are run for both core (CL) and intact polar lipid (IPL) fractions and significant correlations are indicated in bold italics.

	Ring Index	
Parameter	**CL**	**IPL**
pH	***<0.0001***	***<0.0001***
Temp (°C)	***0.0060***	0.34
DO (mg/L)	0.67	0.93
SPC (µS/cm)	0.64	0.10
ORP (mV)	***<0.001***	***0.0019***
Fe^{2+} (mg/L)	***0.018***	***<0.001***
S^{2-} (µg/L)	0.43	0.16

Table S6. Outputs of simple linear regression models for environmental parameters and CL and IPL Ring Index with crenarchaeol from Yellowstone samples. The significance threshold is set to a p-value of 0.05 and significant correlations are indicated in bold italics.

	Ring Index			
	CL		IPL	
Parameter	**p-value**	**adjusted R^2**	**p-value**	**adjusted R^2**
pH	***<0.0001***	0.64	***<0.0001***	0.55
Temp (°C)	***0.0043***	0.17	0.08	0.05
DO (mg/L)	0.38	-0.01	0.76	-0.02
SPC (µS/cm)	0.40	-0.01	0.08	0.05
ORP (mV)	***<0.001***	0.31	***<0.001***	0.31
Fe^{2+} (mg/L)	***0.0042***	0.22	***0.0046***	0.22
S^{2-} (µg/L)	0.97	-0.03	***0.028***	0.11

Table S7. Outputs of 10 multiple linear regression models with highest adjusted R^2 values for environmental parameters and CL Ring Indices with crenarchaeol from Yellowstone samples. The significance threshold is set to 0.05 and significant p-values are indicated in bold italics. Models are listed in order of decreasing adjusted R^2 values.

	Ring Index		
Input Parameters	**p-value**	**Multiple R^2**	**Adjusted R^2**
pH, Temp, DO, Fe^{2+}	***<0.0001***	0.82	0.80
pH, DO, Fe^{2+}	***<0.0001***	0.82	0.79
pH, Temp, DO, Fe^{2+}, S^{2-}	***<0.0001***	0.83	0.79
pH, SPC, DO, Fe^{2+}	***<0.0001***	0.82	0.79
pH, Temp, ORP, DO, Fe^{2+}	***<0.0001***	0.83	0.79
pH, SPC, DO, Fe^{2+}, S^{2-}	***<0.0001***	0.83	0.79
pH, DO, Fe^{2+}, S^{2-}	***<0.0001***	0.82	0.79
pH, Temp, ORP, DO, S^{2-}	***<0.0001***	0.82	0.79
pH, Temp, DO, S^{2-}	***<0.0001***	0.81	0.79
pH, Temp, SPC, DO, Fe^{2+}	***<0.0001***	0.82	0.79

SUPPLEMENTARY INFORMATION

Comparisons of Core and Polar Fractions

To identify whether studies should split GDGTs into CL and IPL fractions, we compared our YNP results for these two fractions. CL and IPL crenarchaeol abundances are strongly positively correlated ($R^2 = 0.81$; Figure S3). Interestingly, the slope of this relationship is 1.5, indicating that on average, crenarchaeol has greater relative abundance in IPL fractions than in CL fractions. IPL lipids are thought to derive from

extant microbial communities and CL lipids record long-term production, indicating that microbial communities in sampled YNP springs may have been producing more crenarchaeol upon collection than the time integral represented in the CL fraction (Lipp and Hinrichs, 2009). Another hypothesis is that crenarchaeol is more labile than the other GDGTs and its CL abundance decreases over time relative to other GDGTs. To distinguish between these two hypotheses, we plotted IPL Ring Index with crenarchaeol versus CL Ring Index with crenarchaeol, which produced a linear trendline with the equation $y = 0.88x + 0.35$ ($R^2 = 0.58$). The result of plotting IPL RI without cren versus CL RI without cren is almost identical with a trendline of $y = 0.88x + 0.34$ ($R^2 = 0.60$). The slopes of 0.88 are close to a 1:1 relationship, different from the crenarchaeol abundance slop of 1.5 for IPL versus CL. This indicates that crenarchaeol may be preferentially degraded compared to other GDGTs with just cyclopentyl rings, supporting the degradation hypothesis over the environmental change hypothesis.

Four sites deviate from the best-fit line and lie outside of the 95% confidence interval in Figure S3, but these outliers maintain a positive relationship between CL and IPL crenarchaeol. The four samples all have relatively high CL and IPL crenarchaeol relative abundances for the Yellowstone dataset. Two sites, Angel Hair (CL = 0.17; IPL = 0.17) and Snow on the Beach (CL = 0.08; IPL = 0.09) have more CL crenarchaeol than predicted by the best-fit line with a slope of 1.5. Both springs have similar relative abundances of crenarchaeol in CL and IPL fractions, indicating the microbes were producing their time-averaged proportion of crenarchaeol at the time of sampling from potentially stable geochemical conditions. Another possibility is that IPL crenarchaeol degradation is enhanced in these springs.

The other two high-abundance sites are Mom's Spaghetti (CL = 0.15; IPL = 0.33) and Bijah Spring (CL = 0.02; IPL = 0.09), which have more IPL crenarchaeol than predicted by the best fit line. The greater relative abundance of IPL crenarchaeol indicates that either the degradation rate of IPL crenarchaeol is lower in these springs, or that the microbial community at the time of sampling of these springs was producing more crenarchaeol relative to other GDGTs than the historical average of this spring. This phenomenon may indicate geochemical conditions that inhibit IPL crenarchaeol degradation, seasonal

variation in environmental parameters that influence crenarchaeol relative abundance, or recent shifts in microbial community or geochemical/geophysical conditions of the springs. Hydrothermal conditions of springs are known to vary with major geyser eruptions, earthquakes, discharge rates, and annual and seasonal disturbances, which could explain these differences in CL and IPL crenarchaeol (Heasler and Jaworowski, 2018).

Conditions experienced by microbes in hot spring environments are also known to be influenced by the volcanic system that drives hydrothermal activity in Yellowstone National Park, which undergoes complex fluctuations over time (Hurwitz and Lowenstern, 2014). Climate variation may also play a role in altering hot spring temperature and chemistry, which would influence trends observed for the 41 Yellowstone samples collected during different times of the year. Variations over even smaller temporal scales can influence hot spring conditions. Across several field seasons, collaborators collected samples from hot springs in Norris Geyser Basin, which is known to have ground temperature variations from ~30 °C to ~50 °C over the course of a single day (Neale et al., 2016). Long-term increases in annual mean air temperature may represent more systemic changes for spring chemistry through indirect processes such as precipitation and nutrient flux, while drought conditions alter input from water sources such as volcanically heated reservoirs, riverine input, and precipitation (Heeter et al., 2021). During the 2022 field season, sediment samples were collected shortly after significant snowfall, which may have influenced spring geochemistry both by direct input and alteration of water table level. Differences in source-water depths of these hydrothermal systems also have important implications for the geochemistry of these springs (Fournier et al., 2002).

The variable conditions of hot springs in Yellowstone may explain discrepancies between crenarchaeol presence/absence in CL and IPL fractions from the same sample. Out of 41 samples generated in this study, eight have detectable levels of CL crenarchaeol and no detectable levels of IPL crenarchaeol (see Excel file of data table). Interestingly, two have detectable levels of IPL crenarchaeol and no detectable levels of CL crenarchaeol. Samples with measurable amounts of CL crenarchaeol and non-detectable IPL

614 crenarchaeol are expected and can be explained by the cessation of crenarchaeol production in these
615 springs with environmental variation or microbial community change because core lipids are degradation
616 products of intact polar lipids. In contrast, the presence of detectable amounts of IPL crenarchaeol and no
617 CL crenarchaeol in two sites is more difficult to explain. One of these sites is a temperature outlier, Cold
618 Sulfur Pool (28.2 °C, pH 2.75), which may have recently begun crenarchaeol production and has a slow
619 degradation rate of archaeal lipids at the relatively low temperature of this spring. The other anomaly,
620 Bubbling Blonde (70 °C, pH 5.02), does not support this slow-degradation interpretation. In Bubbling
621 Blonde the only anomaly is the high dissolved sulfide level, at 7.86 mg L^{-1}. This is the highest value of
622 the Yellowstone dataset, with a second-highest concentration of 2.57 mg L^{-1}. A majority (75%) of samples
623 with S^{2-} data available (36 sites) are at least an order of magnitude lower with an average concentration of
624 700 µg L^{-1}. Upon removal of Bubbling Blonde from this dataset average, the value drops to 496 µg L^{-1}.
625 Sulfide concentration was not measured for Cold Sulfur Pool, which prevents comparison of sulfur
626 abundance across these two sites. However, lipid sulfurization is a known diagenetic process that may
627 lead to enhanced degradation of CL GDGTs in the presence of high sulfur concentrations, which could
628 lead to non-detectable levels of CL crenarchaeol (Schouten et al., 2013; Adam et al., 2000). While there
629 are exceptions, the majority of samples (75.6%) have consistent crenarchaeol presence and absence across
630 CL and IPL fractions.
631
632 The strong linear relationship between CL and IPL crenarchaeol relative abundances justifies plotting
633 results of only CL fraction analyses because similar statistical results are observed for IPL fractions.
634 Multiple linear regression analyses were also run for IPL crenarchaeol to confirm similarity of results
635 with those for CL crenarchaeol reported in Table S3. While results should do not vary between fractions,
636 we chose to plot results for CL crenarchaeol rather than IPL crenarchaeol because CL lipids record a
637 longer history of GDGT production that is not as subject to recent seasonal changes as expected for IPL
638 crenarchaeol (Lipp and Hinrichs, 2009). In addition, we utilized internal GTGT standard to calculate
639 rough absolute abundances of GDGTs in the samples. CL fractions represent the majority of the GDGTs
640 from 94% of samples with internal standard (N = 33), making them preferable for robust quantification on

the QQQ and use in analyses. Two samples, Rabbit Creek Source #2 and Parking Lot Pool had more IPL than CL GDGTs (57% and 84%, respectively), which is anomalous in this dataset. The other 31 samples whose absolute abundance could be calculated had an average percent CL composition of 85.9% ± 13.0, establishing a significant dominance of CL lipids in these samples. The rough calculations from addition of GTGT standard are imprecise and are best suited for order-of-magnitude calculations, which prevents accurate combinations of absolute GDGT abundances from IPL and CL data. Past studies have varied in the lumping or splitting of CL and IPL fractions, so we report compiled literature samples as either total isoprenoid-GDGT abundances or CL abundances (Boyd et al., 2013; Xie et al., 2015). In comparing the literature values to the new data generated in this study, we present only CL crenarchaeol data due to the higher magnitude of CL versus IPL lipid absolute abundances and representation of a long record of GDGT production.

While differences between CL and IPL crenarchaeol abundances can indicate recent shifts in microbial community or environmental conditions in each spring, broad trends of cyclopentyl ring abundances (represented by RI) are consistent across CL and IPL fractions (see Table S4 and Table S5). Given this observation, it may be sufficient to analyze relative GDGT abundances amongst total isoprenoid-GDGTs, rather than splitting into CL and IPL fractions, depending on the scientific goal. This is significant because splitting samples and processing fractions in tandem involves labor intensive wet chemistry protocols and doubles analytical machine time. However, if the environment in question has undergone significant recent changes or researchers are interested in a lipid of high abundance, fraction splitting is suggested to obtain a comprehensive view of lipid production.

Effect of Crenarchaeol on Ring Index Calculations

We compared YNP Ring Index calculated with and without crenarchaeol in Supplemental Figure S4 and demonstrate a strong 1:1 correlation between the two, justifying our utilization of RI calculated with crenarchaeol subsequent analyses. Panels A and C show regressions of YNP samples with detectable

crenarchaeol for CL (R^2 = 0.93) and IPL fractions (R^2 = 0.89), indicating a strong correlation of RI values. The slopes of the significant CL and IPL correlations are 0.98 and 0.88, respectively, which are close to the 1:1 relationship expected for RI values from the same sample. Two samples lie outside of the 95% confidence interval of the regression relationships, which are from Mom's Spaghetti and Angel Hair, the springs with the highest abundances of both CL and IPL crenarchaeol in the Yellowstone dataset (CL = 0.15; IPL = 0.33 and CL = 0.17; IPL = 0.17, respectively). As expected, higher abundances of crenarchaeol increase discrepancies between the two RIs since crenarchaeol contributes four (cyclopentyl) rings to the RI with crenarchaeol. Adding crenarchaeol to the RI of Mom's Spaghetti increased CL RI from 2.71 to 3.06 and IPL from 3.09 to 3.73, while the RI of Angel Hair increased from 1.52 to 2.09 for CL and 1.25 to 1.88 for IPL. These results indicate that incorporating crenarchaeol into RI calculations must be thought through for springs with high concentrations of crenarchaeol.

Depending on the intended purpose of Ring Index, crenarchaeol may best be excluded from RI calculations. In marine sediments, RI can be used to determine whether the TEX_{86} temperature estimates are influenced by factors other than temperature, because Ring Index and TEX_{86} values have a global correlation when temperature is the controlling factor (Zhang et al., 2016). However, if variables other than temperature are more important for ring cyclization, then the relationship between Ring Index and TEX_{86} temperatures fails. Temperature is associated with crenarchaeol distributions, so including crenarchaeol in RI for paleothermometry may be reasonable even if crenarchaeol increases membrane permeability if it can provide a nuanced perspective into GDGT cyclization responses to temperature. If RI is being used to indicate cyclopentyl-forming enzyme activity, crenarchaeol may be included as a four-ringed member. However, if one is using RI as a stress response or indictor of decreased permeability, it may be best to exclude crenarchaeol from ring index, because this lipid prefers moderate temperatures, supporting a membrane-expanding function.

REFERENCES

Adam, P., Schneckenburger, P., Schaeffer, P., & Albrecht, P. (2000). Clues to early diagenetic sulfurization processes from mild chemical cleavage of labile sulfur-rich geomacromolecules. *Geochimica et Cosmochimica Acta*, *64*(20), 3485–3503. https://doi.org/10.1016/S0016-7037(00)00443-9

Albers, S. V., van de Vossenberg, J. L., Driessen, A. J., & Konings, W. N. (2000). Adaptations of the archaeal cell membrane to heat stress. *Frontiers in Bioscience-Landmark*, *5*(3), 813-820.

Amenabar, M. J., & Boyd, E. S. (2018). Mechanisms of Mineral Substrate Acquisition in a Thermoacidophile. *Applied and Environmental Microbiology*, *84*(12), e00334-18. https://doi.org/10.1128/AEM.00334-18f

Becker, K. W., Lipp, J. S., Zhu, C., Liu, X.-L., & Hinrichs, K.-U. (2013). An improved method for the analysis of archaeal and bacterial ether core lipids. *Organic Geochemistry*, *61*, 34–44. https://doi.org/10.1016/j.orggeochem.2013.05.007

Bice, K. L., Birgel, D., Meyers, P. A., Dahl, K. A., Hinrichs, K.-U., & Norris, R. D. (2006). A multiple proxy and model study of Cretaceous upper ocean temperatures and atmospheric CO2 concentrations. *Paleoceanography*, *21*(2). https://doi.org/10.1029/2005PA001203

Blewett, J., Naafs, B. D. A., Gallego-Sala, A. V., & Pancost, R. D. (2020). Effects of temperature and pH on archaeal membrane lipid distributions in freshwater wetlands. *Organic Geochemistry*, *148*, 104080. https://doi.org/10.1016/j.orggeochem.2020.104080

Bligh, E. G., & Dyer, W. J. (1959). A rapid method of total lipid extraction and purification. *Canadian Journal of Biochemistry and Physiology*, *37*(8), 911–917. https://doi.org/10.1139/o59-099

Blum, L. N., Colman, D. R., Eloe-Fadrosh, E. A., Kellom, M., Boyd, E. S., Zhaxybayeva, O., & Leavitt, W. D. (2022). *Distribution and abundance of tetraether lipid cyclization genes in terrestrial hot springs reflects pH* (p. 2022.08.15.504015). bioRxiv. https://doi.org/10.1101/2022.08.15.504015

Boyd, E., Hamilton, T., Wang, J., He, L., & Zhang, C. (2013). The Role of Tetraether Lipid Composition in the Adaptation of Thermophilic Archaea to Acidity. *Frontiers in Microbiology*, *4*. https://www.frontiersin.org/articles/10.3389/fmicb.2013.00062

Boyd, E. S., Pearson, A., Pi, Y., Li, W.-J., Zhang, Y. G., He, L., Zhang, C. L., & Geesey, G. G. (2011). Temperature and pH controls on glycerol dibiphytanyl glycerol tetraether lipid composition in the hyperthermophilic crenarchaeon Acidilobus sulfurireducens. *Extremophiles*, *15*(1), 59–65. https://doi.org/10.1007/s00792-010-0339-y

Boyer, G. M., Schubotz, F., Summons, R. E., Woods, J., & Shock, E. L. (2020). Carbon Oxidation State in Microbial Polar Lipids Suggests Adaptation to Hot Spring Temperature and Redox Gradients. *Frontiers in Microbiology*, *11*. https://www.frontiersin.org/articles/10.3389/fmicb.2020.00229

Brochier-Armanet, C., Boussau, B., Gribaldo, S., & Forterre, P. (2008). Mesophilic crenarchaeota: Proposal for a third archaeal phylum, the Thaumarchaeota. *Nature Reviews Microbiology*, *6*(3), Article 3. https://doi.org/10.1038/nrmicro1852

Burgess, E. A., Unrine, J. M., Mills, G. L., Romanek, C. S., & Wiegel, J. (2012). Comparative Geochemical and Microbiological Characterization of Two Thermal Pools in the Uzon Caldera, Kamchatka, Russia. *Microbial Ecology*, *63*(3), 471–489. https://doi.org/10.1007/s00248-011-9979-4

Church, M. J., Wai, B., Karl, D. M., & DeLong, E. F. (2010). Abundances of crenarchaeal amoA genes and transcripts in the Pacific Ocean. *Environmental Microbiology*, *12*(3), 679–688. https://doi.org/10.1111/j.1462-2920.2009.02108.x

Clayton, T. D., & Byrne, R. H. (1993). Spectrophotometric seawater pH measurements: Total hydrogen ion concentration scale calibration of m-cresol purple and at-sea results. *Deep Sea Research Part I: Oceanographic Research Papers*, *40*(10), 2115–2129. https://doi.org/10.1016/0967-0637(93)90048-8

Cobban, A., Zhang, Y., Zhou, A., Weber, Y., Elling, F. J., Pearson, A., & Leavitt, W. D. (2020). Multiple environmental parameters impact lipid cyclization in Sulfolobus acidocaldarius. *Environmental Microbiology*, *22*(9), 4046–4056. https://doi.org/10.1111/1462-2920.15194

Colman, D. R., Feyhl-Buska, J., Robinson, K. J., Fecteau, K. M., Xu, H., Shock, E. L., & Boyd, E. S. (2016). Ecological differentiation in planktonic and sediment-associated chemotrophic microbial populations in Yellowstone hot springs. *FEMS Microbiology Ecology*, *92*(9), fiw137. https://doi.org/10.1093/femsec/fiw137

Colman, D.R., Keller, L.M., Arteaga-Pozo, E., Andrade-Barahona, E., St. Clair, B., Shoemaker, A., Cox, A., & Boyd, E.S. (2024). Coordination of hot spring geochemistry with microbial genomic diversity, function, and evolution. *Nature Communications*, in press.

Colman, D. R., Lindsay, M. R., Harnish, A., Bilbrey, E. M., Amenabar, M. J., Selensky, M. J., Fecteau, K. M., Debes II, R. V., Stott, M. B., Shock, E. L., & Boyd, E. S. (2021). Seasonal hydrologic and geologic forcing drive hot spring geochemistry and microbial biodiversity. *Environmental Microbiology*, *23*(7), 4034–4053. https://doi.org/10.1111/1462-2920.15617

Colman, D. R., Poudel, S., Hamilton, T. L., Havig, J. R., Selensky, M. J., Shock, E. L., & Boyd, E. S. (2018). Geobiological feedbacks and the evolution of thermoacidophiles. *The ISME Journal*, *12*(1), 225–236. https://doi.org/10.1038/ismej.2017.162

Damer, B., & Deamer, D. (2020). The Hot Spring Hypothesis for an Origin of Life. *Astrobiology*, *20*(4), 429–452. https://doi.org/10.1089/ast.2019.2045

Damsté, J. S. S., Schouten, S., Hopmans, E. C., Duin, A. C. T. van, & Geenevasen, J. A. J. (2002). Crenarchaeol. *Journal of Lipid Research*, *43*(10), 1641–1651. https://doi.org/10.1194/jlr.M200148-JLR200

De La Torre, J. R., Walker, C. B., Ingalls, A. E., Könneke, M., & Stahl, D. A. (2008). Cultivation of a thermophilic ammonia oxidizing archaeon synthesizing crenarchaeol. *Environmental Microbiology*, *10*(3), 810–818. https://doi.org/10.1111/j.1462-2920.2007.01506.x

De Rosa, M., & Gambacorta, A. (1988). The lipids of archaebacteria. *Progress in Lipid Research*, *27*(3), 153–175. https://doi.org/10.1016/0163-7827(88)90011-2

De Rosa, M., Gambacorta, A., Nicolaus, B., Sodano, S., & Bu'Lock, J. D. (1980). Structural regularities in tetraether lipids of Caldariella and their biosynthetic and phyletic implications. *Phytochemistry*, *19*(5), 833–836. https://doi.org/10.1016/0031-9422(80)85121-1

Du, J., Meng, L., Qiu, M., Chen, S., Zhang, B., Song, W., Cong, P., & Zheng, X. (2022). Ammonia-oxidizing archaea and ammonia-oxidizing bacteria communities respond differently in oxy-gen-limited habitats. *Frontiers in Environmental Science*, *10*. https://www.frontiersin.org/articles/10.3389/fenvs.2022.976618

Elling, F. J., Könneke, M., Lipp, J. S., Becker, K. W., Gagen, E. J., & Hinrichs, K.-U. (2014). Effects of growth phase on the membrane lipid composition of the thaumarchaeon *Nitrosopumilus maritimus*

and their implications for archaeal lipid distributions in the marine environment. *Geochimica et Cosmochimica Acta*, *141*, 579–597. https://doi.org/10.1016/j.gca.2014.07.005

Elling, F. J., Könneke, M., Mußmann, M., Greve, A., & Hinrichs, K.-U. (2015). Influence of temperature, pH, and salinity on membrane lipid composition and TEX86 of marine planktonic thaumarchaeal isolates. *Geochimica et Cosmochimica Acta*, *171*, 238–255. https://doi.org/10.1016/j.gca.2015.09.004

Elling, F. J., Könneke, M., Nicol, G. W., Stieglmeier, M., Bayer, B., Spieck, E., de la Torre, J. R., Becker, K. W., Thomm, M., Prosser, J. I., Herndl, G. J., Schleper, C., & Hinrichs, K.-U. (2017). Chemotaxonomic characterisation of the thaumarchaeal lipidome. *Environmental Microbiology*, *19*(7), 2681–2700. https://doi.org/10.1111/1462-2920.13759

Evans, T. W., Könneke, M., Lipp, J. S., Adhikari, R. R., Taubner, H., Elvert, M., & Hinrichs, K.-U. (2018). Lipid biosynthesis of Nitrosopumilus maritimus dissected by lipid specific radioisotope probing (lipid-RIP) under contrasting ammonium supply. *Geochimica et Cosmochimica Acta*, *242*, 51–63. https://doi.org/10.1016/j.gca.2018.09.001

Feyhl-Buska, J., Chen, Y., Jia, C., Wang, J.-X., Zhang, C. L., & Boyd, E. S. (2016). Influence of Growth Phase, pH, and Temperature on the Abundance and Composition of Tetraether Lipids in the Thermoacidophile Picrophilus torridus. *Frontiers in Microbiology*, *7*. https://doi.org/10.3389/fmicb.2016.01323

Fournier, R. O., Weltman, U., Counce, D., White, L. D., & Janik, C. J. (2002). Results of weekly chemical and isotopic monitoring of selected springs in Norris Geyser Basin, Yellowstone National Park during June-September, 1995. In *Results of weekly chemical and isotopic monitoring of selected springs in Norris Geyser Basin, Yellowstone National Park during June-September, 1995* (USGS Numbered Series No. 2002–344; Open-File Report, Vols. 2002–344, p. 50). U.S. Geological Survey. https://doi.org/10.3133/ofr02344

Gabriel, J. L., & Lee Gau Chong, P. (2000). Molecular modeling of archaebacterial bipolar tetraether lipid membranes. *Chemistry and Physics of Lipids*, *105*(2), 193–200. https://doi.org/10.1016/S0009-3084(00)00126-2

Grossman, E. L., & Joachimski, M. M. (2022). Ocean temperatures through the Phanerozoic reassessed. *Scientific Reports*, *12*(1), 8938. https://doi.org/10.1038/s41598-022-11493-1

Harvey, H. R., Fallon, R. D., & Patton, J. S. (1986). The effect of organic matter and oxygen on the degradation of bacterial membrane lipids in marine sediments. *Geochimica et Cosmochimica Acta*, *50*(5), 795–804. https://doi.org/10.1016/0016-7037(86)90355-8

He, L., Zhang, C. L., Dong, H., Fang, B., & Wang, G. (2012). Distribution of glycerol dialkyl glycerol tetraethers in Tibetan hot springs. *Geoscience Frontiers*, *3*(3), 289–300. https://doi.org/10.1016/j.gsf.2011.11.015

Heasler, H., & Jaworowski, C. (2018). Hydrothermal monitoring of Norris Geyser Basin, Yellowstone National Park, USA, using airborne thermal infrared imagery. *Geothermics*, *72*, 24–46. https://doi.org/10.1016/j.geothermics.2017.10.016

Heeter, K. J., Rochner, M. L., & Harley, G. L. (2021). Summer Air Temperature for the Greater Yellowstone Ecoregion (770–2019 CE) Over 1,250 Years. *Geophysical Research Letters*, *48*(7), e2020GL092269. https://doi.org/10.1029/2020GL092269

Huguet, C., Hopmans, E. C., Febo-Ayala, W., Thompson, D. H., Sinninghe Damsté, J. S., & Schouten, S. (2006). An improved method to determine the absolute abundance of glycerol dibiphytanyl glycerol

tetraether lipids. *Organic Geochemistry*, *37*(9), 1036–1041. https://doi.org/10.1016/j.orggeochem.2006.05.008

Hurley, S. J., Elling, F. J., Könneke, M., Buchwald, C., Wankel, S. D., Santoro, A. E., Lipp, J. S., Hinrichs, K.-U., & Pearson, A. (2016). Influence of ammonia oxidation rate on thaumarchaeal lipid composition and the TEX86 temperature proxy. *Proceedings of the National Academy of Sciences*, *113*(28), 7762–7767. https://doi.org/10.1073/pnas.1518534113

Hurley, S. J., Lipp, J. S., Close, H. G., Hinrichs, K.-U., & Pearson, A. (2018). Distribution and export of isoprenoid tetraether lipids in suspended particulate matter from the water column of the Western Atlantic Ocean. *Organic Geochemistry*, *116*, 90–102. https://doi.org/10.1016/j.orggeochem.2017.11.010

Hurwitz, S., & Lowenstern, J. B. (2014). Dynamics of the Yellowstone hydrothermal system. *Reviews of Geophysics*, *52*(3), 375–411. https://doi.org/10.1002/2014RG000452

James, C., & Lytle, D. (2004). *Relationships between Oxidation-Reduction Potential , Oxidant , and pH in Drinking Water*. https://www.semanticscholar.org/paper/Relationships-between-Oxidation-Reduction-Potential-James-Lytle/81f84a82fb386e8d03057e6df7f107e9e86b983d

Jia, C., Zhang, C. L., Xie, W., Wang, J.-X., Li, F., Wang, S., Dong, H., Li, W., & Boyd, E. S. (2014). Differential temperature and pH controls on the abundance and composition of H-GDGTs in terrestrial hot springs. *Organic Geochemistry*, *75*, 109–121. https://doi.org/10.1016/j.orggeochem.2014.06.009

Jiang, L.-Q., Carter, B. R., Feely, R. A., Lauvset, S. K., & Olsen, A. (2019). Surface ocean pH and buffer capacity: Past, present and future. *Scientific Reports*, *9*(1), Article 1. https://doi.org/10.1038/s41598-019-55039-4

Justnes, H. (2020). Transformation Kinetics of Burnt Lime in Freshwater and Sea Water. *Materials*, *13*. https://doi.org/10.3390/ma13214926

Kaur, G., Mountain, B. W., Stott, M. B., Hopmans, E. C., & Pancost, R. D. (2015). Temperature and pH control on lipid composition of silica sinters from diverse hot springs in the Taupo Volcanic Zone, New Zealand. *Extremophiles*, *19*(2), 327–344. https://doi.org/10.1007/s00792-014-0719-9

Kim, J.-H., Schouten, S., Hopmans, E. C., Donner, B., & Sinninghe Damsté, J. S. (2008). Global sediment core-top calibration of the TEX86 paleothermometer in the ocean. *Geochimica et Cosmochimica Acta*, *72*(4), 1154–1173. https://doi.org/10.1016/j.gca.2007.12.010

Kim, J.-H., van der Meer, J., Schouten, S., Helmke, P., Willmott, V., Sangiorgi, F., Koç, N., Hopmans, E. C., & Damsté, J. S. S. (2010). New indices and calibrations derived from the distribution of crenarchaeal isoprenoid tetraether lipids: Implications for past sea surface temperature reconstructions. *Geochimica et Cosmochimica Acta*, *74*(16), 4639–4654. https://doi.org/10.1016/j.gca.2010.05.027

Konings, W. N., Albers, S.-V., Koning, S., & Driessen, A. J. M. (2002). The cell membrane plays a crucial role in survival of bacteria and archaea in extreme environments. *Antonie van Leeuwenhoek*, *81*(1), 61–72. https://doi.org/10.1023/A:1020573408652

Kuypers, M. M. M., Blokker, P., Erbacher, J., Kinkel, H., Pancost, R. D., Schouten, S., & Sinninghe Damsté, J. S. (2001). Massive Expansion of Marine Archaea During a Mid-Cretaceous Oceanic Anoxic Event. *Science*, *293*(5527), 92–95. https://doi.org/10.1126/science.1058424

Li, F., Zhang, C. L., Dong, H., Li, W., & Williams, A. (2013). Environmental controls on the distribution of archaeal lipids in Tibetan hot springs: Insight into the application of organic proxies for

biogeochemical processes. *Environmental Microbiology Reports*, *5*(6), 868–882. https://doi.org/10.1111/1758-2229.12089

Lipp, J. S., & Hinrichs, K.-U. (2009). Structural diversity and fate of intact polar lipids in marine sediments. *Geochimica et Cosmochimica Acta*, *73*(22), 6816–6833. https://doi.org/10.1016/j.gca.2009.08.003

Liu, X., Lipp, J. S., & Hinrichs, K.-U. (2011). Distribution of intact and core GDGTs in marine sediments. *Organic Geochemistry*, *42*(4), 368–375. https://doi.org/10.1016/j.orggeochem.2011.02.003

Lloyd, C. T., Iwig, D. F., Wang, B., Cossu, M., Metcalf, W. W., Boal, A. K., & Booker, S. J. (2022). Discovery, structure and mechanism of a tetraether lipid synthase. *Nature*, *609*(7925), Article 7925. https://doi.org/10.1038/s41586-022-05120-2

Macalady, J. L., Vestling, M. M., Baumler, D., Boekelheide, N., Kaspar, C. W., & Banfield, J. F. (2004). Tetraether-linked membrane monolayers in Ferroplasma spp: A key to survival in acid. *Extremophiles*, *8*(5), 411–419. https://doi.org/10.1007/s00792-004-0404-5

National Institute of Standard and Technology. 4.1.4.4. LOESS (aka LOWESS) - Introduction to Process Modeling - Engineering Statistics Handbook. *NIST.gov.* https://www.itl.nist.gov/div898/handbook/pmd/section1/pmd144.htm

Neale, C. M. U., Jaworowski, C., Heasler, H., Sivarajan, S., & Masih, A. (2016). Hydrothermal monitoring in Yellowstone National Park using airborne thermal infrared remote sensing. *Remote Sensing of Environment*, *184*, 628–644. https://doi.org/10.1016/j.rse.2016.04.016

Oger, P. M., & Cario, A. (2013). Adaptation of the membrane in Archaea. *Biophysical Chemistry*, *183*, 42–56. https://doi.org/10.1016/j.bpc.2013.06.020

Palmer, M. R., Pearson, P. N., & Cobb, S. J. (1998). Reconstructing Past Ocean pH-Depth Profiles. *Science*, *282*(5393), 1468–1471. https://doi.org/10.1126/science.282.5393.1468

Pancost, R. D., Pressley, S., Coleman, J. M., Talbot, H. M., Kelly, S. P., Farrimond, P., Schouten, S., Benning, L., & Mountain, B. W. (2006). Composition and implications of diverse lipids in New Zealand Geothermal sinters. *Geobiology*, *4*(2), 71–92. https://doi.org/10.1111/j.1472-4669.2006.00069.x

Paraiso, J. J., Williams, A. J., Huang, Q., Wei, Y., Dijkstra, P., Hungate, B., Dong, H., Hedlund, B., & Zhang, C. (2013). The distribution and abundance of archaeal tetraether lipids in U.S. Great Basin hot springs. *Frontiers in Microbiology*, *4*. https://www.frontiersin.org/articles/10.3389/fmicb.2013.00247

Pearson, A., Huang, Z., Ingalls, A. E., Romanek, C. S., Wiegel, J., Freeman, K. H., Smittenberg, R. H., & Zhang, C. L. (2004). Nonmarine Crenarchaeol in Nevada Hot Springs. *Applied and Environmental Microbiology*, *70*(9), 5229–5237. https://doi.org/10.1128/AEM.70.9.5229-5237.2004

Pearson, A., Pi, Y., Zhao, W., Li, W., Li, Y., Inskeep, W., Perevalova, A., Romanek, C., Li, S., & Zhang, C. L. (2008). Factors Controlling the Distribution of Archaeal Tetraethers in Terrestrial Hot Springs. *Applied and Environmental Microbiology*, *74*(11), 3523–3532. https://doi.org/10.1128/AEM.02450-07

Pearson, A., & Ingalls, A. E. (2013). Assessing the Use of Archaeal Lipids as Marine Environmental Proxies. *Annual Review of Earth and Planetary Sciences*, *41*(1), 359–384. https://doi.org/10.1146/annurev-earth-050212-123947

Pitcher, A., Hopmans, E. C., Mosier, A. C., Park, S.-J., Rhee, S.-K., Francis, C. A., Schouten, S., & Sinninghe Damsté, J. S. (2011). Core and Intact Polar Glycerol Dibiphytanyl Glycerol Tetraether Lipids of Ammonia-Oxidizing Archaea Enriched from Marine and Estuarine Sediments. *Applied and Environmental Microbiology*, *77*(10), 3468–3477. https://doi.org/10.1128/AEM.02758-10

Pitcher, A., Rychlik, N., Hopmans, E. C., Spieck, E., Rijpstra, W. I. C., Ossebaar, J., Schouten, S., Wagner, M., & Sinninghe Damsté, J. S. (2010). Crenarchaeol dominates the membrane lipids of Candidatus Nitrososphaera gargensis, a thermophilic Group I.1b Archaeon. *The ISME Journal*, *4*(4), 542–552. https://doi.org/10.1038/ismej.2009.138

Pitcher, A., Schouten, S., & Sinninghe Damsté, J. S. (2009). In Situ Production of Crenarchaeol in Two California Hot Springs. *Applied and Environmental Microbiology*, *75*(13), 4443–4451. https://doi.org/10.1128/AEM.02591-08

Qin, W., Carlson, L. T., Armbrust, E. V., Devol, A. H., Moffett, J. W., Stahl, D. A., & Ingalls, A. E. (2015). Confounding effects of oxygen and temperature on the TEX86 signature of marine Thaumarchaeota. *Proceedings of the National Academy of Sciences*, *112*(35), 10979–10984. https://doi.org/10.1073/pnas.1501568112

R Core Team (2024). R: A language and environment for statistical computing. *R Foundation for Statistical Computing.* https://www.r-project.org/

Ren, M., Feng, X., Huang, Y., Wang, H., Hu, Z., Clingenpeel, S., Swan, B. K., Fonseca, M. M., Posada, D., Stepanauskas, R., Hollibaugh, J. T., Foster, P. G., Woyke, T., & Luo, H. (2019). Phylogenomics suggests oxygen availability as a driving force in Thaumarchaeota evolution. *The ISME Journal*, *13*(9), Article 9. https://doi.org/10.1038/s41396-019-0418-8

Robert, F., & Chaussidon, M. (2006). A palaeotemperature curve for the Precambrian oceans based on silicon isotopes in cherts. *Nature*, *443*(7114), Article 7114. https://doi.org/10.1038/nature05239

Schouten, S., Hopmans, E. C., Pancost, R. D., & Damsté, J. S. S. (2000). Widespread occurrence of structurally diverse tetraether membrane lipids: Evidence for the ubiquitous presence of low-temperature relatives of hyperthermophiles. *Proceedings of the National Academy of Sciences*, *97*(26), 14421–14426. https://doi.org/10.1073/pnas.97.26.14421

Schouten, S., Hopmans, E. C., Schefuß, E., & Sinninghe Damsté, J. S. (2002). Distributional variations in marine crenarchaeotal membrane lipids: A new tool for reconstructing ancient sea water temperatures? *Earth and Planetary Science Letters*, *204*(1), 265–274. https://doi.org/10.1016/S0012-821X(02)00979-2

Schouten, S., Hopmans, E. C., & Sinninghe Damsté, J. S. (2013). The organic geochemistry of glycerol dialkyl glycerol tetraether lipids: A review. *Organic Geochemistry*, *54*, 19–61. https://doi.org/10.1016/j.orggeochem.2012.09.006

Schouten, S., van der Meer, M. T. J., Hopmans, E. C., Rijpstra, W. I. C., Reysenbach, A.-L., Ward, D. M., & Sinninghe Damsté, J. S. (2007). Archaeal and Bacterial Glycerol Dialkyl Glycerol Tetraether Lipids in Hot Springs of Yellowstone National Park. *Applied and Environmental Microbiology*, *73*(19), 6181–6191. https://doi.org/10.1128/AEM.00630-07

Sinninghe Damsté, J. S., Rijpstra, W. I. C., Hopmans, E. C., den Uijl, M. J., Weijers, J. W. H., & Schouten, S. (2018). The enigmatic structure of the crenarchaeol isomer. *Organic Geochemistry*, *124*, 22–28. https://doi.org/10.1016/j.orggeochem.2018.06.005

Sinninghe Damsté, J. S., Rijpstra, W. I. C., Hopmans, E. C., Jung, M.-Y., Kim, J.-G., Rhee, S.-K., Stieglmeier, M., & Schleper, C. (2012). Intact Polar and Core Glycerol Dibiphytanyl Glycerol

Tetraether Lipids of Group I.1a and I.1b Thaumarchaeota in Soil. *Applied and Environmental Microbiology*, *78*(19), 6866–6874. https://doi.org/10.1128/AEM.01681-12

Sinninghe Damsté, J. S., Schouten, S., Hopmans, E. C., Duin, A. C. T. van, & Geenevasen, J. A. J. (2002). Crenarchaeol. *Journal of Lipid Research*, *43*(10), 1641–1651. https://doi.org/10.1194/jlr.M200148-JLR200

Slonczewski, J. L., Fujisawa, M., Dopson, M., & Krulwich, T. A. (2009). Cytoplasmic pH Measurement and Homeostasis in Bacteria and Archaea. In R. K. Poole (Ed.), *Advances in Microbial Physiology* (Vol. 55, pp. 1–317). Academic Press. https://doi.org/10.1016/S0065-2911(09)05501-5

Stahl, D. A., & de la Torre, J. R. (2012). Physiology and Diversity of Ammonia-Oxidizing Archaea. *Annual Review of Microbiology*, *66*(1), 83–101. https://doi.org/10.1146/annurev-micro-092611-150128

Taylor, K. W. R., Huber, M., Hollis, C. J., Hernandez-Sanchez, M. T., & Pancost, R. D. (2013). Re-evaluating modern and Palaeogene GDGT distributions: Implications for SST reconstructions. *Global and Planetary Change*, *108*, 158–174. https://doi.org/10.1016/j.gloplacha.2013.06.011

Tierney, J. E. (2012). GDGT Thermometry: Lipid Tools for Reconstructing Paleotemperatures. *The Paleontological Society Papers*, *18*, 115–132. https://doi.org/10.1017/S1089332600002588

Touati, D. (2000). Iron and oxidative stress in bacteria. *Archives of Biochemistry and Biophysics*, *373*(1), 1–6. https://doi.org/10.1006/abbi.1999.1518

Tourte, M., Schaeffer, P., Grossi, V., & Oger, P. M. (2022). Membrane adaptation in the hyperthermophilic archaeon Pyrococcus furiosus relies upon a novel strategy involving glycerol monoalkyl glycerol tetraether lipids. *Environmental Microbiology*, *24*(4), 2029–2046. https://doi.org/10.1111/1462-2920.15923

Valentine, D. L. (2007). Adaptations to energy stress dictate the ecology and evolution of the Archaea. *Nature Reviews Microbiology*, *5*(4), Article 4. https://doi.org/10.1038/nrmicro1619

van de Vossenberg, J. L., Driessen, A. J., & Konings, W. N. (1998). The essence of being extremophilic: The role of the unique archaeal membrane lipids. *Extremophiles: Life Under Extreme Conditions*, *2*(3), 163–170. https://doi.org/10.1007/s007920050056

Weber, Y., Sinninghe Damsté, J. S., Hopmans, E. C., Lehmann, M. F., & Niemann, H. (2017). Incomplete recovery of intact polar glycerol dialkyl glycerol tetraethers from lacustrine suspended biomass. *Limnology and Oceanography: Methods*, *15*(9), 782–793. https://doi.org/10.1002/lom3.10198

White, D. C., Davis, W. M., Nickels, J. S., King, J. D., & Bobbie, R. J. (1979). Determination of the Sedimentary Microbial Biomass by Extractible Lipid Phosphate. *Oecologia*, *40*(1), 51–62.

Wu, W., Zhang, C., Wang, H., He, L., Li, W., & Dong, H. (2013). Impacts of temperature and pH on the distribution of archaeal lipids in Yunnan hot springs, China. *Frontiers in Microbiology*, *4*. https://www.frontiersin.org/articles/10.3389/fmicb.2013.00312

Xie, W., Zhang, C. L., Wang, J., Chen, Y., Zhu, Y., de la Torre, J. R., Dong, H., Hartnett, H. E., Hedlund, B. P., & Klotz, M. G. (2015). Distribution of ether lipids and composition of the archaeal community in terrestrial geothermal springs: Impact of environmental variables. *Environmental Microbiology*, *17*(5), 1600–1614. https://doi.org/10.1111/1462-2920.12595

Yang, Y., Zhang, C., Lenton, T. M., Yan, X., Zhu, M., Zhou, M., Tao, J., Phelps, T. J., & Cao, Z. (2021). The Evolution Pathway of Ammonia-Oxidizing Archaea Shaped by Major Geological Events. *Molecular Biology and Evolution*, *38*(9), 3637–3648. https://doi.org/10.1093/molbev/msab129

Zeng, Z., Liu, X.-L., Farley, K. R., Wei, J. H., Metcalf, W. W., Summons, R. E., & Welander, P. V. (2019). GDGT cyclization proteins identify the dominant archaeal sources of tetraether lipids in the ocean. *Proceedings of the National Academy of Sciences*, *116*(45), 22505–22511. https://doi.org/10.1073/pnas.1909306116

Zeng, Z., Chen, H., Yang, H., Chen, Y., Yang, W., Feng, X., Pei, H., & Welander, P. V. (2022). Identification of a protein responsible for the synthesis of archaeal membrane-spanning GDGT lipids. *Nature Communications*, *13*(1), Article 1. https://doi.org/10.1038/s41467-022-29264-x

Zhang, C. L., Pearson, A., Li, Y.-L., Mills, G., & Wiegel, J. (2006). Thermophilic Temperature Optimum for Crenarchaeol Synthesis and Its Implication for Archaeal Evolution. *Applied and Environmental Microbiology*, *72*(6), 4419–4422. https://doi.org/10.1128/AEM.00191-06

Zhang, Y. G., Pagani, M., & Wang, Z. (2016). Ring Index: A new strategy to evaluate the integrity of TEX86 paleothermometry. *Paleoceanography*, *31*(2), 220–232. https://doi.org/10.1002/2015PA002848

Zhao, W., Song, Z., Jiang, H., Li, W., Mou, X., Romanek, C. S., Wiegel, J., Dong, H., & Zhang, C. L. (2011). Ammonia-oxidizing Archaea in Kamchatka Hot Springs. *Geomicrobiology Journal*, *28*(2), 149–159. https://doi.org/10.1080/01490451003753076

Zhou, A., Weber, Y., Chiu, B. K., Elling, F. J., Cobban, A. B., Pearson, A., & Leavitt, W. D. (2020). Energy flux controls tetraether lipid cyclization in Sulfolobus acidocaldarius. *Environmental Microbiology*, *22*(1), 343–353. https://doi.org/10.1111/1462-2920.14851